Equilibrium of a Shallow Arch Subjected to PZT Actuators and a Deadweight Load

by

Nitish Singh

Thesis submitted to the Faculty of the

Virginia Polytechnic Institute and State University

in partial fulfillment of the requirements for the degree of

MASTER OF SCIENCE

IN

AEROSPACE ENGINEERING

APPROVED:

E. R. Johnson, Chair

R. Kapania

Z. Chaudhry

August 22, 1996.

Blacksburg, Virginia

Keywords: shallow, arch, panel, piezoelectric, snap-through

EQUILIBRIUM OF A SHALLOW ARCH SUBJECTED TO PZT ACTUATORS AND A DEADWEIGHT LOAD

by

Nitish Singh

E. R. Johnson, Chairman

Aerospace and Ocean Engineering

(ABSTRACT)

The geometrically nonlinear response of a shallow, circular, cylindrical panel under a midspan line load and induced strain actuation is presented. The panel is a laminate of piezoelectric material perfectly bonded to the convex and concave surfaces of a core of passive material. Since the curved edges are free and the straight edges are pinned a fixed distance apart, the response of the panel is independent of the axial coordinate. Hence, the governing ordinary differential equations are of the same form as for a shallow circular arch. Without induced strain actuation, the panel exhibits snap-through behavior under the midspan load. Induced strain distributions are determined at a constant midspan load to displace the panel to an inverted configuration in a stable manner. This adaptive structure may find application as an electromechanical, nonlinear spring with a digital-like, load-displacement response characteristic.

Acknowledgments

It is with deepest gratitude that I thank my advisor, Dr. E. R. Johnson, for his guidance and advice during my stay at Virginia Tech. The understanding and patience he has demonstrated during the tougher times of this research is greatly appreciated. His innumerable reviews of this manuscript has been of immense value. It has indeed been a pleasure working with Dr. Johnson and I am glad he was my advisor.

I also appreciate the time and effort spent by Dr. Zaffir Chaudhry in helping me understand the technical concepts of smart materials. Despite his absence from Virginia Tech., he has been of great assistance. I would like to thank Dr. R. Kapania for agreeing to serve on my committee. A special word of thanks to Dr. R. H. Plaut for being kind enough to serve on my examining committee at a very short notice.

I take this opportunity to thank my friends Radhika Rajgopal and Gautam Rajan for their warm support that saw me through my rougher moments. Nicolas Guyot deserves a mention for being a great friend and for making life a lot more cheerful in the lab with his fine sense of humor. Last but not the least, I would like to thank my parents, Indu and Harjit Singh, whose love and support made these two years seem a lot more easier for me. I thank them for always standing by me and believing in me. This thesis is dedicated to them.

Table of Contents

List of figures

List of tables

1. Introduction

Curvature can be used to enhance the performance of piezoelectric actuators[1]. Curved structures and piezoelectric actuators are considered in this study for application as an electromechanical, nonlinear spring with a digital-like, load-displacement response characteristic. This electromechanical spring is simply a solid state actuator material bonded to the concave and convex sides of a shallow circular cylindrical panel. The panel core is made of a passive material. See Figure 1.1. The ideal response of this electromechanical device is a large displacement occurring at a constant value of the load as shown in Figure 1.1. The top and the bottom piezoelectric layers of this laminated panel are polarized in the thickness direction. Thus, a direct current electric field applied in the thickness direction to the top and bottom piezoelectric layers, through voltages V_b and V_t, induce circumferential forces in the panel in addition to those resulting from the midspan

load P. A non-linear spring characteristic of this type has been proposed for the control of wing shape to improve the aerodynamic and aeroelastic performance of fixed wing and rotary wing aircraft[2]. Whether a piezoelectric controlled non-linear spring can be used in a large scale application like a airplane wings is questionable.

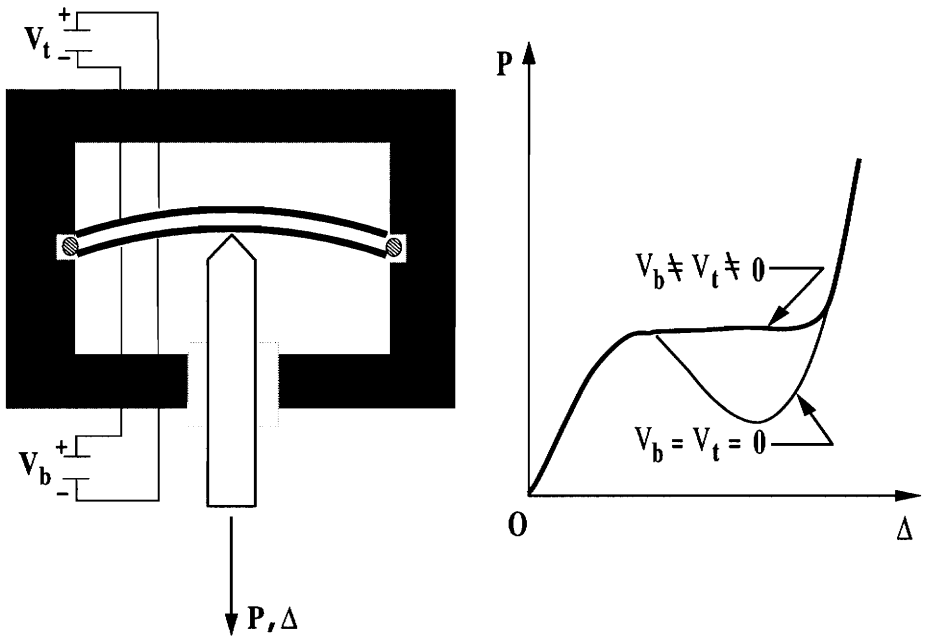

Figure 1.1 An electromechanical nonlinear spring with digital-like load displacement response.

However, the results from this theoretical study can be used to provide limits on the force-displacement performance achievable with this electromechanical nonlinear spring.

A shallow curved panel under a downward deadweight load P at midspan, without actuator control, exhibits snap-through instability at either a limit point or at bifurcation point on the load-displacement equilibrium response plot. The loss of stability of the equilibrium state is dynamic, since no stable adjacent equilibrium state is in the vicinity of the critical equilibrium state. The objective of this work is to determine if induced strain actuators can be used to find a stable alternate equilibrium path from a configuration near the critical one on the ascending portion of the load-displacement plot to an inverted configuration at the same load. See Figure 1.1. This is a structure under multiple independent loads V_t, V_b and P, where V_t and V_b are the actuation loads in the top and bottom actuators, respectively. These loads can be represented as a point in a three dimensional load space spanned by three Cartesian axes V_t, V_b and P. In the load space, the objective is to find a path for V_t and V_b in a P = constant plane such that the arch displaces through stable equilibrium states to an inverted configuration.

This is a study of the geometrically nonlinear response of a shallow, cylindrical panel laminated with a piezoelectric material. Hence, in the following two sections of this chapter, the snap-through phenomenon is reviewed first, followed by a review of adaptive structures using piezoelectric materials.

1.1 Shallow shells/arches

A shell is considered shallow if it's middle surface does not deviate much from a plane. Consider an orthogonal Cartesian coordinate system x, y, z in a given space in which the middle surface is denoted by the equation

$$z = z(x, y) \tag{1.1}$$

Then, the shell would be defined as shallow if the conditions

$$\left(\frac{\partial z}{\partial x}\right)^2 << 1 \tag{1.2}$$

and

$$\left(\frac{\partial z}{\partial y}\right)^2 << 1 \tag{1.3}$$

are satisfied everywhere on the middle surface.

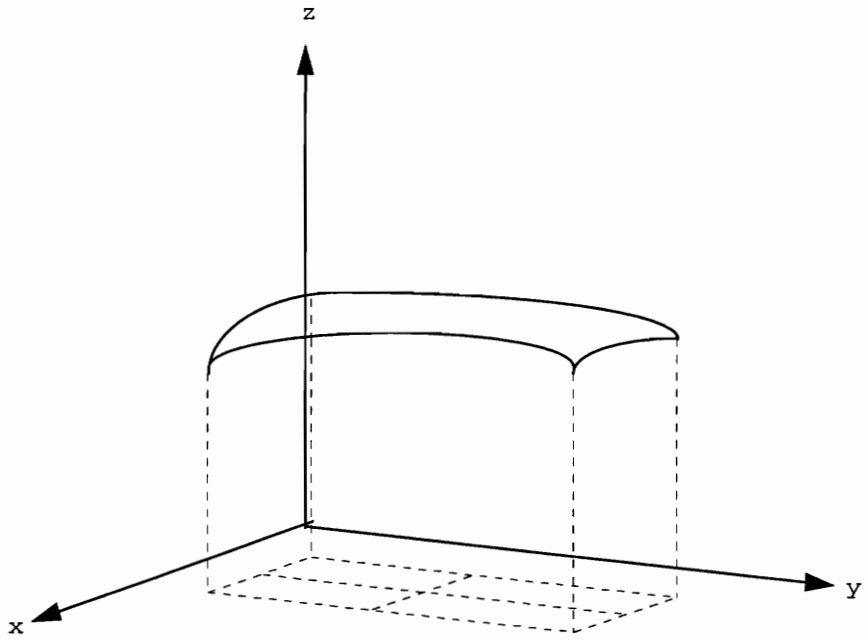

Figure 1.2. Representation of a shallow shell in a Cartesian coordinates

In this study, we are concerned with a circular cylindrical panel which is both shallow and thin at the same time. For a cylindrical panel, the conditions given by eq. (1.2) and eq. (1.3) are written as

$$\left(\frac{\partial z}{\partial x}\right)^2 = 0 \tag{1.4}$$

and

$$\left(\frac{\partial z}{\partial y}\right)^2 << 1 \tag{1.5}$$

A parametric form of the middle surface of the panel shown in Figure 1.3 is

$$(x, y, z) = \left(x, RSin(\theta), R\left(Cos(\theta) - Cos(\beta)\right)\right) \tag{1.6}$$

where R denotes the radius of the middle surface, θ the polar angle, and β denotes the semi-opening angle; $-\beta \le \theta \le +\beta$. Thus,

$$\frac{dz}{dy} = \frac{dz}{d\theta}\frac{d\theta}{dy} = Tan(\theta) \tag{1.7}$$

and the condition given in eq. (1.5) is satisfied if θ is small in magnitude. Since the maximum magnitude of θ is β, the condition in eq. (1.5) is satisfied if β is small. Alternatively, a shallow panel is also characterized by a small rise to span ratio. Let $z(0) = H$ denote the maximum rise of the panel above a horizontal line through its end points, and let L denote the span, or horizontal distance between the end points. Then,

$$H = R(1 - Cos(\beta))$$

$$L = 2RSin(\beta) \tag{1.8}$$

and the rise-to-span ratio is

$$\left(\frac{H}{L}\right) = \frac{1}{2}\left(\frac{1 - Cos(\beta)}{Sin(\beta)}\right) \tag{1.9}$$

If β is small, then

$$\left(\frac{H}{L}\right) \approx \left(\frac{1}{4}\right)\beta \tag{1.10}$$

so that small values of β correspond to a small rise-to-span ratio. A shallow, circular cylindrical panel is characterized by a small semi-opening angle. Note that shallowness is independent of the radius R.

In addition, a thin shell is characterized by small thickness to the radius ratio h/R (Figure 1.3.). In general, a shell is thin if $0 < h/R < 1/20$. In this work a shallow, thin circular cylindrical panel is the focus problem.

If the geometry, boundary conditions, load and material properties are uniform along the x-direction, then the response of the panel is a function of the circumferential coordinate θ only. The equations governing the response of the shallow cylindrical panel are of the same form as those governing a shallow arch. In the sequel, the cylindrical panel is referred to as an arch for this reason.

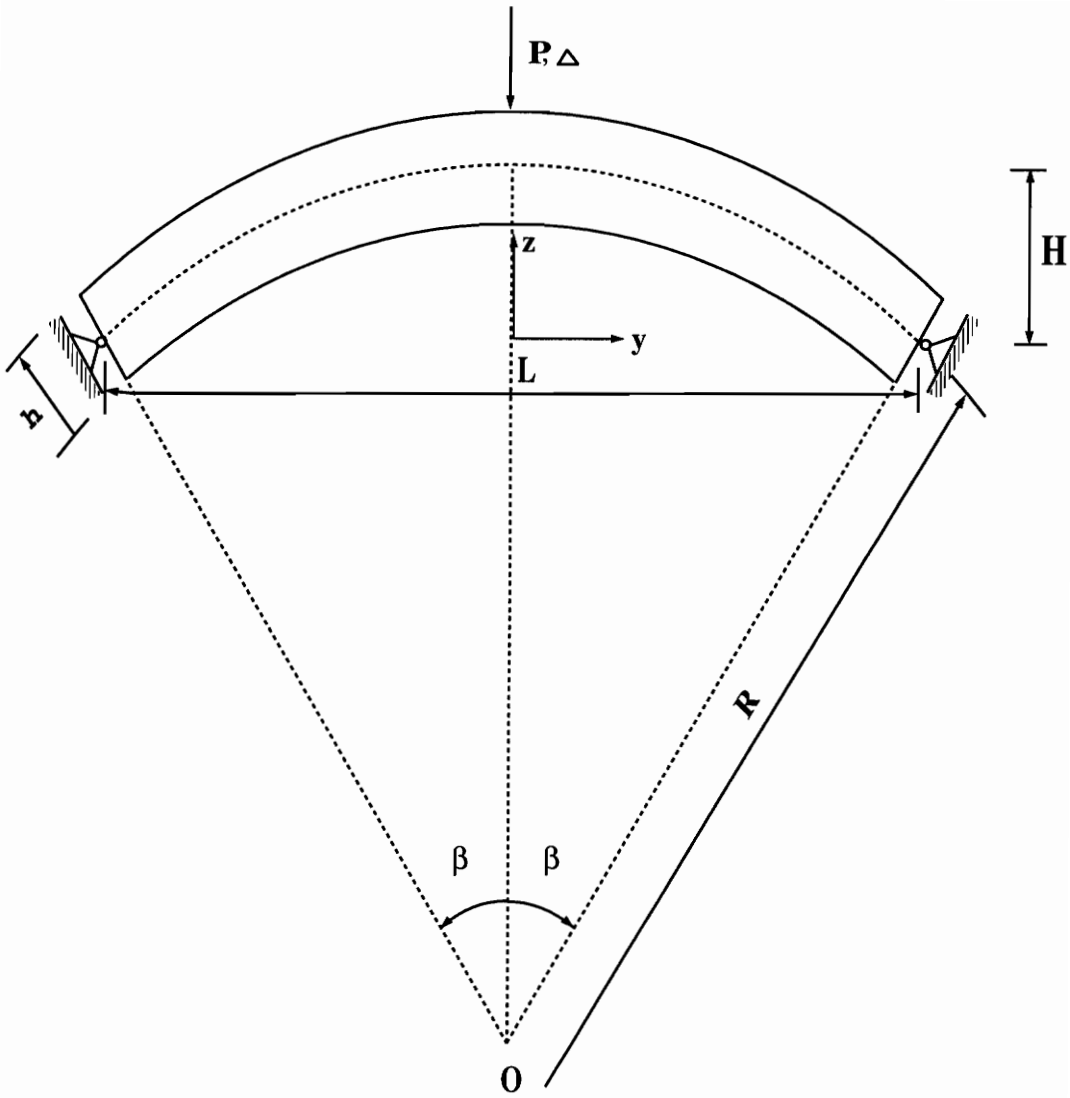

Figure 1.3. Geometry of a shallow panel, or arch

1.2 Instabilities associated with shallow arches

Structural stability is one of the major considerations in the design of light and thin structures. Generally these structures are desirable for the savings in the fabrication, construction and service life costs. Aerospace structures, which are slender and at the same time designed to satisfy strength requirements, are the most obvious examples of the use of light and thin members.

The shallow arch is one of the simplest structures capable of demonstrating most of the features of elastic instability theory.

1.2.1 Snap-through of shallow circular arch

Consider a shallow circular panel, or arch, subjected to a downward deadweight line load of intensity P at the midspan. The ends of the panel are simply supported and held a fixed distance apart. See Figure 1.3. The downward midspan displacement is denoted by Δ. It will be shown in Chapter 2, that the behavior of the load-displacement response is governed by a single dimensionless parameter λ defined by

$$\lambda^4 = \frac{\left(AR^2\beta^4\right)}{D} \tag{1.11}$$

where A designates the extensional stiffness and D the bending stiffness of the panel in the circumferential direction. For a panel wall made of an isotropic and homogenous material, these stiffnesses are given by

$$A = \frac{Eh}{\left(1 - \nu^2\right)} \tag{1.12}$$

and

$$D = \frac{1}{12}\frac{Eh^3}{\left(1 - \nu^2\right)} \tag{1.13}$$

where E denotes the modulus of elasticity, ν the Poisson's ratio, and h denotes the thickness of the arch. Then, for an isotropic material arch, the parameter λ reduces to

$$\lambda^4 = 48\left(\frac{H}{h}\right)^2 \tag{1.14}$$

and larger values of λ correspond to a deeper arch.

For a pin-ended, circular arch under a mid-span load, the qualitative behavior is governed by the parameter λ[3]. For $0 < \lambda < 1.9762$, the load-deflection behavior is monotonic and there is no snap through. See Figure 1.4(a). For $1.9762 < \lambda < 2.825$, the load-deflection response exhibits a limit point (relative maximum load). Since there is no stable adjacent equilibrium state, when the load is increased from the limit point, the arch will snap-through dynamically to a stable inverted equilibrium configuration. See Figure 1.4(b). For $\lambda > 2.825$, an asymmetric bifurcation point occurs on the ascending portion of the P-Δ plot, and snap-through occurs at the bifurcation point. A bifurcation point is the intersection of two equilibrium paths, and the secondary path intersecting the primary path corresponds to asymmetric configurations of the arch. (The primary path corresponds to symmetric equilibrium configurations about the mid-span). Bifurcation behavior is shown in Figure 1.4(c), where the additional axis, labeled b in the plot, represents a generalized displacement that is a measure of the asymmetry in the shape of the deflected arch.

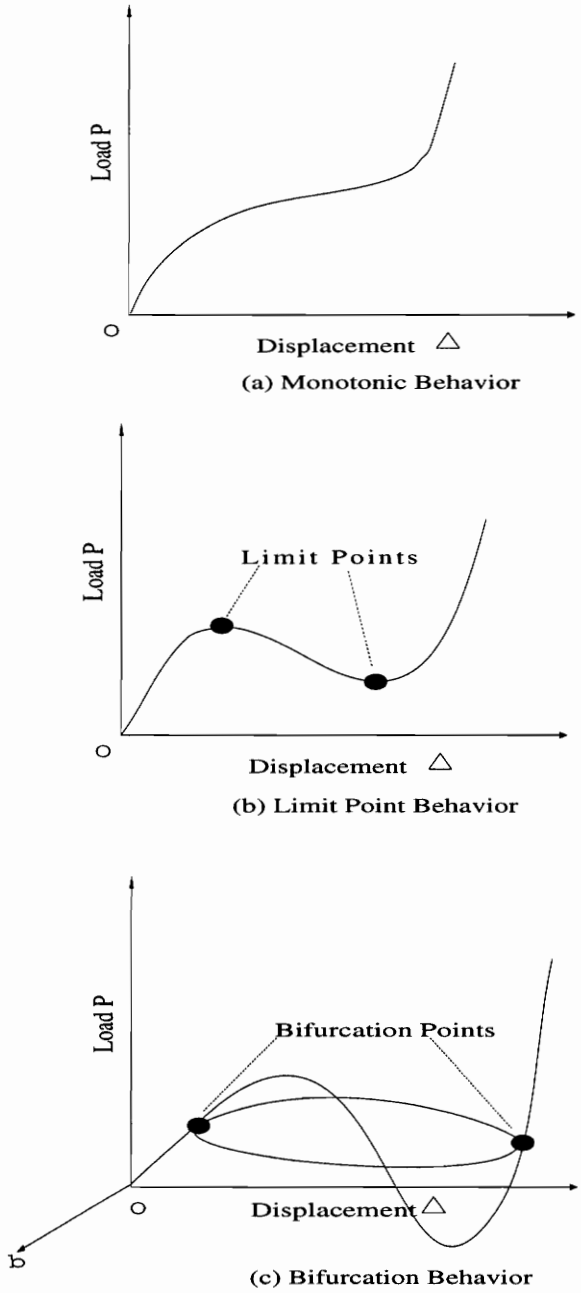

Figure 1.4. Load-displacement responses for a shallow circular arch with pinned ends held a fixed distance apart and subjected to a downward mid-span load *P*.

It is possible to design a nonlinear spring with a digital-like load response characteristic using a shallow arch with monotonic load response $\{0 < \lambda < 1.9762\}$ and no active materials. However, these are very shallow arches with limited load capacity. We seek to increase the design space to larger load capacities by considering deeper arches. Deeper arches, as mentioned above, are prone to snap-through instability. Thus, a means to stabilize the response is needed, and the use of active materials is one possibility worth investigating.

1.2.2 Previous work on buckling of shallow arches

Biezeno[4] studied the response of a shallow arch with fixed pinned ends subjected to a concentrated load acting at the midspan. Using a shallow curved beam solution and a series solution, he analyzed the symmetric response of a shallow arch. Symmetry, here, was defined with respect to the midspan location of the arch. However, Biezeno presented no results concerning the asymmetric response.

Fung and Kaplan[5] later conducted a more thorough investigation into the behavior of shallow arches, specifically, the case of an initially sinusoidal arch using a series solution. They investigated the asymmetric displacement mode in greater detail than Biezeno.

Shreyer and Masur[6] performed an identical study on circular arches with clamped ends. They determined the equilibrium behavior of the structure and also analyzed the stability of the equilibrium states. In their study, the initial rise-to-span ratio determined whether the buckling occurred at the limit point on the primary path or at the bifurcation point on the primary path. Their investigations of the finite deformation behavior of the shallow arch were restricted to isotropic and homogeneous materials with elastic behavior. They did not consider load eccentricity or geometric imperfections.

Later Shreyer[7] presented an analysis of the effects of the initial imperfections on the response of shallow circular arches with clamped ends which showed that the arch is an imperfection sensitive structure. Plaut[8] performed a more thorough investigation into the effects of load positioning on shallow circular arches with pinned ends. Different behaviors were observed due to load offsets. However, only those arches which showed a loss of stability at the bifurcation points when the load was at midspan were found to be sensitive to load eccentricity. Plaut[9,10,11] also investigated the stability of shallow arches under three independent concentrated loads. The stability boundaries in the three-dimensional loading space are surfaces that separate regions of stable and unstable loading configurations. It was found that bifurcation instability on a loading ray (proportional loading) is only possible in a certain plane in the loading space, and that the stability boundaries exhibit cusps at bifurcation points.

In addition to the research papers cited above many other studies of both shallow and deep arches of various shapes, subjected to various loadings and boundary conditions are reported in the texts by Timoshenko and Gere[12], Simitses[13], and Dym[14]. In spite of the extensive literature on the geometrically nonlinear response and snap-through of shallow arches, no references were found on stabilizing the large displacement response using piezoelectric materials. Even in cases where piezoelectric materials have been combined with shells, rings and arches, the emphasis has mostly been on dynamic analysis[15] described by linear response equations. Some of the work done in static analysis of shells is presented in References16,17,18,19.

1.3 Adaptive structures

The precision performance required of future space structures has motivated a new approach to structural design which involves a greater and more important role for control systems and sensory and actuating systems. Structures with sensors can perceive changes

in their environment. These structures are known as sensory structures. The presence of actuators in a structure enable it to alter the system characteristics in a controlled manner. Such structures are called adaptive structures. The combination of sensory structures with adaptive structures yields the controlled structure which has capabilities of both of these.

In this study we restrict ourselves to adaptive structures. Adaptive structures allow for geometric or property changes to take place to yield a configuration more compatible with the immediate environment of the structure. Such structures do not possess a sensory system. The advancement in the field of adaptive structures has been made possible primarily due the development of a class of materials known as intelligent materials.

1.3.1 Intelligent materials

Some materials have certain properties which can be used to perform a function in a structure. These properties of the material can be enhanced to provide additional functionality. When these material properties are combined with functions related to information and automation science like sensing, memory processing and others, an intelligent material is created. An intelligent material, therefore, is a material capable of sensing and responding to an external stimuli like a force or an electric field. This response is communicated to the substructure to which it is coupled in order to produce the desired change in geometry or property.

A number of intelligent materials are presently available. These include piezoceramics, shape memory alloys, optical fibers, electro-rhealogical fluids, magnetostrictive materials and electrostrictive materials. The advancement of these materials was primarily due to a desire to reduce structural weight. Hence, these materials have the potential to replace the conventional mechanical controlling devices. One of the most widely used intelligent material is the piezoelectric material.

1.3.2 Piezoelectric materials

Piezoelectric materials generate a mechanical response when subjected to an electric field and conversely produce an electric response under the action of a mechanical stress. One of the most commonly used piezoelectric materials is PZT (lead-zirconate-titanate). The PZT can be used as an actuator and a sensor. It is a ceramic and hence, it can be made into thin sheets and can be adhered to almost any surface. They are available in a variety of shapes.

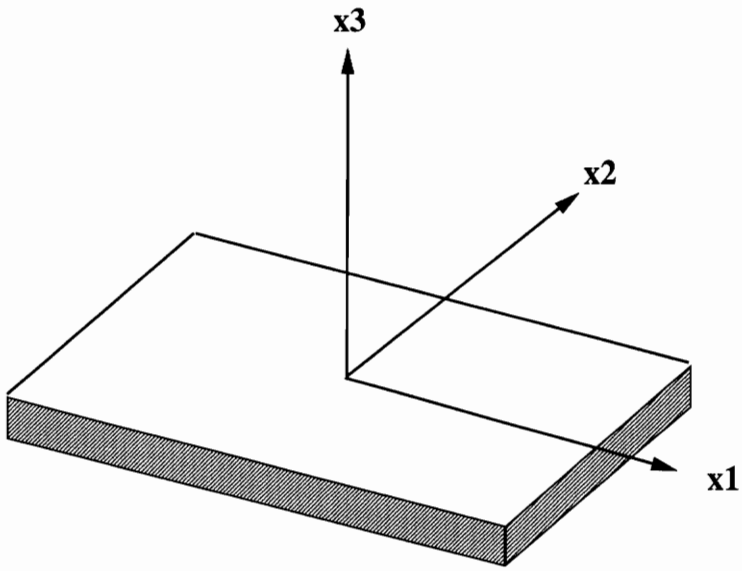

Figure 1.5. PZT orientation in the Cartesian Plane

During the manufacture of PZTs, they are polarized by applying a large electric field across them. This causes the crystallites to become oriented in the direction of the applied

field. This direction is referred to as the poling direction and is designated as the x_3 axis in Cartesian coordinates x_1, x_2 and x_3. Once the PZT has been polarized, it behaves as a transversely isotropic material with x_1-x_2 plane as the plane of isotropy. As the PZT is extremely thin in the x_3 direction, the elongation mainly occurs in the x_1-x_2 plane and elongation can be neglected in the x_3 direction. Therefore, the induced strains are primarily in the x_1-x_2 plane.

The free induced strain, Λ, is related to the electric field, E, and the piezoelectric coefficient, d, of the PZT by the relation

$$\Lambda = Ed \tag{1.15}$$

The applied electric field can be expressed in terms of the applied voltage, V, and the PZT thickness, t, as

$$E = \frac{V}{t} \tag{1.16}$$

Therefore, the induced strain, Λ, is dependent on the PZT thickness, t, as shown by the following relation

$$\Lambda = \frac{Vd}{t} \tag{1.17}$$

Hence, for a particular value of the applied voltage, the induced strain produced by the PZT is inversely proportional to its thickness, i.e., a thinner PZT produces larger induced strains.

1.3.3 Long-stroke actuators

The major drawback of piezoelectric materials is their limited stroke or displacement. Though PZTs are generally used as single layer actuators, they can also be used in a multilayer configuration. The multilayer configuration induces greater forces and moments on the substructure. In other words, the actuator stroke can be increased by making multilayer or stacked devices in which each element adds to the effect. Stacked PZTs operate mechanically in series and electrically in parallel.

1.3.4 Developments in long-stroke actuators

The field of large stroke actuators is attracting considerable interest. The prime motive is to develop an actuator which is capable of producing a larger displacement and more force. Niino[20] et al have developed an electrostatic actuator capable of producing a propulsive force of 21 N with a ± 1000V excitation voltage. It consists of a stack of ten actuators[21] and is equipped with a position sensor placed in a closed loop. It is capable of reaching peak values of 1.2 W of mechanical power.

Bamford[22] et al have developed a long stroke actuator which uses six piezoelectric stacks. This device has been designed for motions of up to 2000 μm. The key feature of this device is its capability of operating at reduced performance with varying degrees of failure within the actuator. It is capable of producing both high frequency small stroke and low frequency large stroke.

Another promising technology being developed is by Gene Haertling[22], Bishop Distinguished Professor at the Clemson University. He developed a method to transform the PZT-family piezoceramic wafers into dome or saddle-shaped structures which

exhibited a hundred fold improvement in response. These wafers are called Rainbow (for reduced and internally biased oxide wafers). These Rainbow wafers range in size from 0.5 to 2.0 inches long and have a thickness ranging from 0.01 to 0.03 inches. These can move as much as 0.05 inches at applied voltages 300 - 500 V. An eight element stack can achieve a stroke of up to 0.20 inches.

Another long-stroke actuator has been developed by Richard Helbaum[23] at NASA Langley. This actuator is based on a piezoelectric ceramic wafer attached to a metal backing with a polyimide adhesive. It is called Thunder (for thin-layer composite unimorph ferroelectric driver and sensor). This device works on a mismatch of the coefficient of thermal expansion between the ceramic and the metal. Such a wafer with a diameter of 7.0 cm has produced a maximum displacement of 1.0 cm with no load on it.

1.4 Objective

The objective of this study is to find stable equilibrium paths for a shallow arch subjected to induced strains and a downward, deadweight load at midspan. The arch is circular with pinned ends held at a fixed distance apart. Piezoelectric material is bonded to the convex and concave surfaces of the arch. Without PZT actuation, the arch exhibits snap-through instability under the midspan load. We would like to determine induced strain distributions that provide an alternate stable equilibrium path from the original configuration to the inverted configuration of the arch.

1.5 Outline

In chapter 2, the equations for a shallow, circular cylindrical panel with perfectly bonded actuators are developed. Both the equilibrium equations and the stability equations for the

arch are derived in detail. Chapter 3 introduces the approach adopted in selecting the actuation strain distribution for displacing the arch to an inverted configuration using an alternate stable equilibrium path. The strategy developed in chapter 3 is used to obtain numerical results for specific arches, or for specific λ-values, in chapter 4. Finally, chapter 5 provides a summary, concluding remarks and suggestions for future work in this area.

2. Formulation

2.1 Geometric configuration

The coordinate system and configuration of the arch is shown in Figure. 2.1. The radius of the middle surface of the arch is denoted by R, the thickness of each PZT layer is denoted by t_1, and the core thickness is denoted by t_2. The total thickness of the arch $h = 2t_1 + t_2$. The semi-opening angle of the arch is denoted by β. The position through the thickness of the configuration is denoted by the coordinate ζ, which is positive away from the center of curvature. At the middle surface $\zeta = 0$. The arch rise, denoted by H, is the vertical distance measured at the midspan from the line joining the two ends of the arch. The arch is simply supported by smooth hinges at each end, and the ends remain a fixed distance,

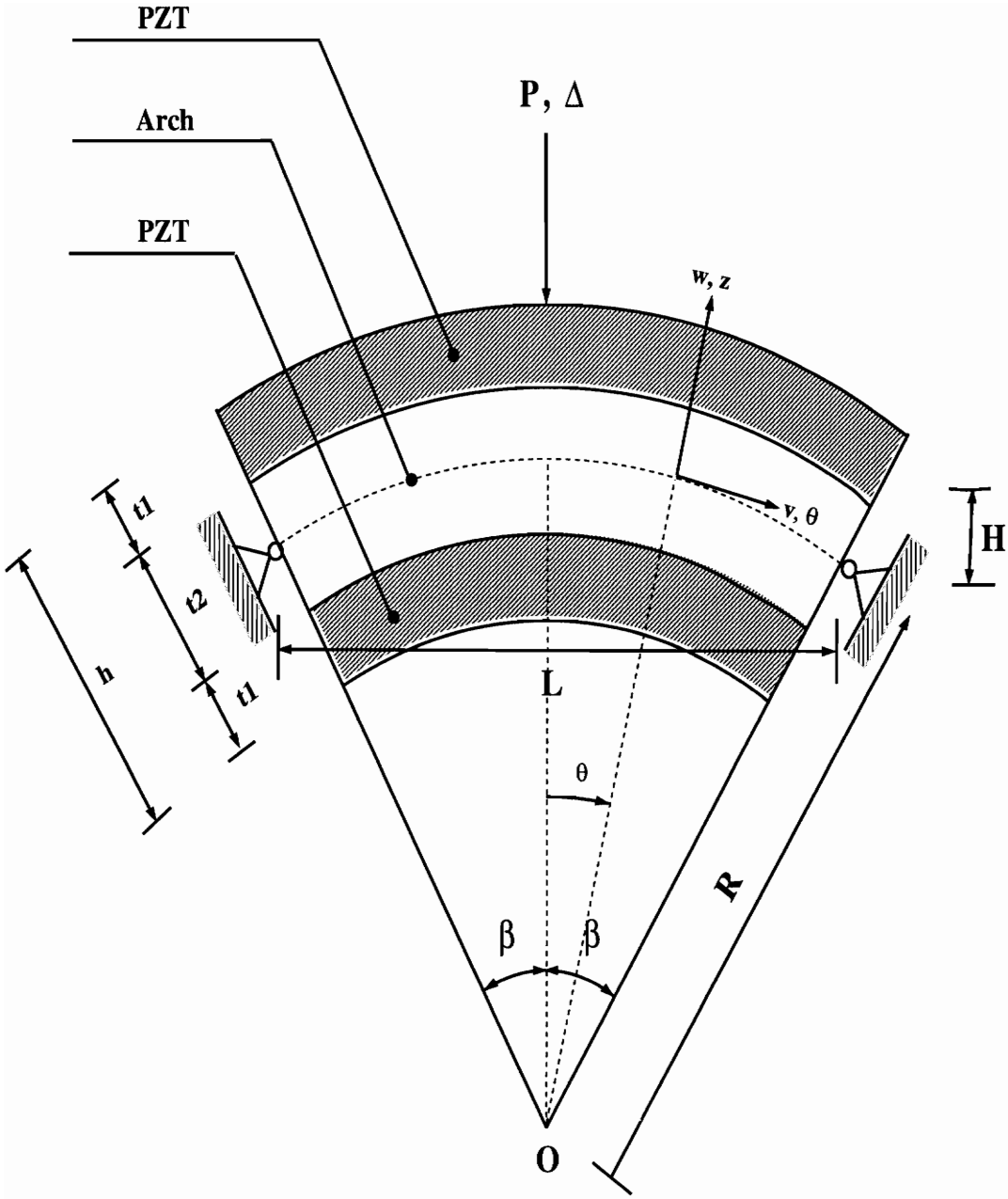

Figure 2.1. Geometric configuration of a shallow arch

L, apart. The radial displacement is designated by w and the tangential displacement is denoted by v. The dead weight line load P acts downwards at the midspan.

Apart from assuming the response of a the arch as a function of the circumferential coordinate θ only, the other assumptions include linear elastic material behavior and that the panel is thin enough so that the transverse shear strains and transverse normal stresses are negligible compared to the in-plane stresses and strains.

2.2 Derivation of the governing equations

The arch depicted in Figure 2.1, is actually a long cylindrical panel. That is, the cross-section is rectangular with the depth into the page being much larger than the thickness, h. The formulation of the governing equilibrium equations of this panel are identical in form to a shallow circular arch, so the terms arch and panel are used interchangeably. The response of the panel is independent of the axial coordinate, x, since the geometry, boundary conditions at $\theta = \pm\beta$, material properties and mid-span line load P are uniform in the x-direction. Let the axial, circumferential and normal displacements of the middle surface be denoted by u, v and w respectively. Since the arch, or panel, response is independent of the x coordinate, we have

$$u(x,\theta) = 0$$

$$v(x,\theta) = v(\theta)$$

$$w(x,\theta) = w(\theta) \tag{2.1}$$

For this form of the displacement field, the parallel surface strains of the classical shell

theory are

$$\varepsilon_x = 0$$

$$\varepsilon_\theta = \varepsilon + \zeta\kappa$$

$$\gamma_{x\theta} = 0 \tag{2.2}$$

where ε denotes the circumferential normal strain, and κ the change of the normal curvature of the middle surface. For the geometrically non-linear shallow shell theory, ε and κ are related to the displacements by

$$\varepsilon = \frac{1}{R}\frac{dv}{d\theta} + \frac{1}{R}w + \frac{1}{2}\left(\frac{1}{R}\frac{dw}{d\theta}\right)^2$$

$$\kappa = -\frac{1}{R^2}\frac{d^2w}{d\theta^2} \tag{2.3}$$

Equilibrium of the structure is enforced using the principle of virtual work, written as

$$\delta W_{ext} = \delta W_{\text{int}} \tag{2.4}$$

where the internal and external virtual work per unit axial length of the panel are

$$\delta W_{\text{int}} = \int_{-\beta}^{+\beta} (N\delta\varepsilon + M\delta\kappa) R d\theta$$

$$\delta W_{ext} = -P\delta w(0) \tag{2.5}$$

The circumferential stress resultant and the stress couple are defined in terms of the circumferential normal stress σ_θ by

$$(N, M) = \int_{-\frac{h}{2}}^{+\frac{h}{2}} (1, \zeta)\sigma_\theta d\zeta \tag{2.6}$$

The equilibrium equations, boundary conditions, and the transition conditions at the point of load application, can then be obtained using the principle of virtual work. The equilibrium equation associated with virtual displacement δv is

$$\frac{dN}{d\theta} = 0 \tag{2.7}$$

and the equilibrium equation associated with the virtual displacement δw is

$$-\frac{1}{R^2}\frac{d^2M}{d\theta^2} - \frac{d}{d\theta}\left(\frac{1}{R}\frac{dw}{d\theta}N\right) + N = 0 \tag{2.8}$$

The associated boundary conditions for the pinned, fixed ends are

$$v(\pm\beta) = 0$$

$$w(\pm\beta) = 0$$

$$M(\pm\beta) = 0 \tag{2.9}$$

and the transition conditions at $\theta = 0$ are

$$v, w, \frac{dw}{d\theta}, N, M \text{ continuous}$$

$$\left[\frac{1}{R}\frac{dw}{d\theta}N + \frac{1}{R}\frac{dM}{d\theta}\right]_{0-}^{0+} = P \tag{2.10}$$

As shown in Figure 2.1, the arch is composed of PZT layers bonded to the core. The material law is developed from a general, linear electroelastic constitutive equation. The arch material is assumed to be orthotropic in the (x, θ, ζ) coordinate system with the thickness normal stress $\sigma_\zeta = 0$. The electroelastic constitutive equations for the in-plane strains are

$$\begin{bmatrix} \varepsilon_x \\ \varepsilon_\theta \\ \gamma_{x\theta} \end{bmatrix} = \begin{bmatrix} \frac{1}{E_x} & -\frac{\nu_{\theta x}}{E_\theta} & 0 \\ -\frac{\nu_{x\theta}}{E_x} & \frac{1}{E_\theta} & 0 \\ 0 & 0 & \frac{1}{G_{x\theta}} \end{bmatrix} \begin{bmatrix} \sigma_x \\ \sigma_\theta \\ \sigma_{x\theta} \end{bmatrix} + \begin{bmatrix} d_{31} \\ d_{31} \\ 0 \end{bmatrix} E_3 \tag{2.11}$$

where E_x and E_θ are the moduli of elasticity, $\nu_{x\theta}$ is the major Poisson's ratio, $\nu_{\theta x}$ $(=\nu_{x\theta}E_\theta/E_x)$ is the minor Poisson's ratio, $G_{x\theta}$ is the shear modulus, d_{31} is the piezoelectric strain coefficient and E_3 is the electric field. According to eq. (2.2), the strains ε_x and $\gamma_{x\theta}$ vanish for a response independent of the axial coordinate, x, so that the material law for the stress is

$$\sigma_\theta = Q\left[\varepsilon_\theta - (1 + \nu_{x\theta})\Lambda\right] \tag{2.12}$$

where the reduced stiffness $Q_1 = E_\theta/(1-\nu_{\theta x}\nu_{x\theta})$, and the induced strain, $\Lambda_t = d_{31}E_3$, is as defined in the earlier chapter. Equation. (2.12) is specialized for the laminated construction of PZT material bonded to the core as shown in Figure 2.1. For the case of polarization in the ζ - direction, the PZT material is isotropic in the x-θ plane so that $E_x = E_\theta = E_a$, say, and $\nu_{x\theta} = \nu_{\theta x} = \nu_a$. The core is a passive material but is taken to be orthotropic and homogeneous. Thus, the material law as a function of ζ becomes

$$\sigma_\theta = Q_1\left[\varepsilon_\theta - (1+\nu_a)\Lambda_t\right] \qquad \frac{t_2}{2} < \zeta < \frac{h}{2}$$

$$\sigma_\theta = Q_2\varepsilon_\theta \qquad -\frac{t_2}{2} < \zeta < \frac{t_2}{2}$$

$$\sigma_\theta = Q_1\left[\varepsilon_\theta - (1+\nu_a)\Lambda_b\right] \qquad -\frac{h}{2} < \zeta < -\frac{t_2}{2} \tag{2.13}$$

where $Q_1 = E_a/\left(1-\nu_a^2\right)$, Q_2 is the core's reduced stiffness, Λ_t is the induced strain in the top actuator and, Λ_b is the induced strain in the bottom actuator. The strain ε_θ from the second of the eqs. (2.2) is substituted in eqs. (2.13) and these are then introduced into the resultant definitions given by eqs. (2.6). As a result of these substitutions, eqs. (2.6) become explicit in ζ and are integrated through the thickness of the panel to get

$$N = A\varepsilon - A_1\left(\Lambda_b + \Lambda_t\right)$$

$$M = D\kappa + B_1\left(\Lambda_b - \Lambda_t\right) \tag{2.14}$$

where the laminate stiffnesses are defined by

$$A = 2Q_1 t_1 + Q_2 t_2$$

$$A_1 = Q_1 (1 + v_a) t_1$$

$$D = \frac{Q_1}{12}\left[h^3 - t_2^3\right] + \frac{Q t_2^3}{12}$$

$$B_1 = \frac{Q_1}{8}(1 + v_a)\left[h^2 - t_2^2\right] \tag{2.15}$$

The governing differential equations in terms of the normal displacement $w(\theta)$ and circumferential resultant N are obtained as follows: Equilibrium eq. (2.7) shows that N is spatially uniform. Using the first of the eqs. (2.14), the first strain-displacement equation in eq. (2.3) and the boundary condition given by eq. (2.9) for v, the circumferential resultant is integrated over the panel to get

$$N = \frac{A}{2\beta}\int_{-\beta}^{+\beta}\left(\frac{1}{R}w + \frac{1}{2R^2}\left(\frac{dw}{d\theta}\right)^2\right)d\theta - A_1(\Lambda_b + \Lambda_t) \tag{2.16}$$

The curvature-displacement relation from the second of the eqs. (2.3) is then substituted in the second of the constitutive equations given by eqs. (2.14). This result is then substituted for the moment resultant in the equilibrium eqs. (2.8) to get

$$\frac{D}{R^4}\frac{d^4 w}{d\theta^4} - \frac{N}{R}\frac{d^2 w}{d\theta^2} + N = 0 \tag{2.17}$$

The remaining boundary conditions of eq. (2.9) lead to

$$w(\pm\beta) = 0$$

$$-\frac{D}{R^2}\frac{d^2w}{d\theta^2}\bigg|_{\theta=\pm\beta} + B_1(\Lambda_b - \Lambda_t) = 0 \tag{2.18}$$

and the transition conditions of eq. (2.10) at $\theta = 0$ remaining to be satisfied are

$$w, \frac{dw}{d\theta}, \frac{d^2w}{d\theta^2} \quad \text{continuous and} \quad -\frac{d^3w}{d\theta^3}\bigg|_{0-}^{0+} = \frac{PR^3}{D} \tag{2.19}$$

Scaled variables are introduced. These are defined as

$$\Gamma = \frac{\theta}{\beta}$$

$$\phi = -\frac{w}{R\beta^2}$$

$$\eta = -\frac{N}{A\beta^2} \tag{2.20}$$

Note that $\phi(0) \approx 1$ if $w(0) = -H$, which corresponds to the center displacement of an inverted configuration of the arch. In terms of these dimensionless variables, eqs. (2.16-2.18) become

$$\frac{1}{\lambda^4}\frac{d^4\phi}{d\Gamma^4} + \eta\left(1 + \frac{d^2\phi}{d\Gamma^2}\right) = 0 \tag{2.21}$$

$$\phi = \phi(\Gamma) \qquad\qquad 0 < |\Gamma| < 1$$

$$\eta = \frac{1}{2}\int_{-1}^{+1}\left(\phi - \frac{1}{2}\left(\frac{d\phi}{d\Gamma}\right)^2\right)d\Gamma + e_a \tag{2.22}$$

$$\phi(\pm 1) = 0 \qquad\qquad \left.\frac{d^2\phi}{d\Gamma^2}\right|_{\Gamma=\pm 1} + e_b = 0 \tag{2.23}$$

At $\Gamma = 0$, the transition conditions of eq. (2.19) become

$$\phi, \frac{d\phi}{d\Gamma}, \frac{d^2\phi}{d\Gamma^2} \quad \text{continuous and} \quad \left.\frac{d^3\phi}{d\Gamma^3}\right|_{0-}^{0+} = p\lambda^4 \tag{2.24}$$

The additional quantities appearing in the eqs. (2.21-2.24) are the dimensionless arch rise parameter, which has been defined in the previous chapter, and is given by

$$\lambda^4 = \frac{AR^2\beta^4}{D} \tag{2.25}$$

the actuation load parameters

$$e_a = \frac{A_1}{A\beta^2}(\Lambda_b + \Lambda_t)$$

$$e_b = \frac{B_1 R}{D}(\Lambda_b - \Lambda_t) \tag{2.26}$$

and the midspan load parameter

$$p = \frac{P}{A\beta^3} \tag{2.27}$$

For a panel made of an isotropic and homogeneous material, $A = Eh/(1-\nu^2)$ and $D = Eh^3/\left(12\left(1-\nu^2\right)\right)$, so that the arch rise parameter reduces to $\lambda^4 = 48(H/h)^2$. Thus, larger values of λ correspond to a deeper arch.

2.3 Derivation of the stability equations

The mechanical system considered here is conservative since the material is elastic and the induced strains and the midspan load are independent of the displacement of the arch. The strain energy can be obtained by substituting the material law given by eqs. (2.14) into the eq. (2.5) for internal virtual work and noting the first variation of the functional

$$U = \frac{1}{2}\int_{-\beta}^{+\beta}\left[A\varepsilon^2 - 2A_1\left(\Lambda_t + \Lambda_b\right)\varepsilon + D\kappa^2 - 2B_1\left(\Lambda_t - \Lambda_b\right)\kappa\right]Rd\theta \tag{2.28}$$

is the same as the internal virtual work. Functional U is the strain energy per unit length in the x-direction. For the deadweight line load P, the external potential per unit length in the x-direction is given by the

$$V = Pw(0) \tag{2.29}$$

The total potential energy per unit length in the x-direction is then given by

$$\Pi = U + V \tag{2.30}$$

The stability equations are derived from the Trefftz criterion, which is a stationarity condition for the second variation of the total potential energy about the equilibrium state. In order to obtain the second variation of the total potential energy, let

$$v(\theta) \rightarrow v(\theta) + v_1(\theta)$$

$$w(\theta) \rightarrow w(\theta) + w_1(\theta) \tag{2.31}$$

where the displacements denoted by $v(\theta)$ and $w(\theta)$ on the right hand side of the eqs. (2.31) are those of the equilibrium state. Substituting these displacements of eqs. (2.31) into the eq. (2.30) and arranging the terms in the ascending powers of the displacements v_1 and w_1 yields

$$\Pi[v + v_1, w + w_1] = \Pi[v, w] + \delta^2\Pi + \delta^2\Pi \ \ldots\ldots\ldots \tag{2.32}$$

or

$$\Delta\Pi = \Pi[v + v_1, w + w_1] - \Pi[v, w] = \delta^2\Pi + \delta^2\Pi \ \ldots\ldots \tag{2.33}$$

where $\delta\Pi$ is a linear functional in v_1 and w_1 which is equal to zero because displacements v and w are those of the equilibrium state, and $\delta^2\Pi$ is a quadratic functional in v_1 and w_1 representing the second variation in the total potential energy. The second variation is

$$\delta^2\Pi = \frac{1}{2}\int_{-\beta}^{+\beta}\left(A\varepsilon_1^2 + 2N\varepsilon_2 + D\kappa_1^2\right)Rd\theta \tag{2.34}$$

where the additional strains about the equilibrium state are given as

$$\varepsilon_1 = \frac{1}{R}\left(\frac{dv_1}{d\theta} + w_1\right) + \frac{1}{R^2}\frac{dw}{d\theta}\frac{dw_1}{d\theta} \tag{2.35}$$

$$\varepsilon_2 = \frac{1}{2R^2}\left(\frac{dw_1}{d\theta}\right)^2 \tag{2.36}$$

$$\kappa_1 = -\frac{1}{R^2}\left(\frac{d^2 w_1}{d\theta^2}\right) \tag{2.37}$$

The mathematical statement of Trefftz criterion is

$$\delta\left(\delta^2\Pi\right) = 0 \tag{2.38}$$

for the critical equilibrium state where the outer variation is with respect to v_1 and w_1. The first variation of the quadratic functional $\delta^2\Pi$, thus, leads to the Euler equations or the stability equations and the associated boundary conditions. The stability equations are obtained as

$$-\frac{1}{R}\frac{dN_1}{d\theta} = 0 \tag{2.39}$$

$$\frac{1}{R^2}\frac{d^2 M_1}{d\theta^2} + \frac{d}{d\theta}\left(\frac{N}{R^2}\frac{dw_1}{d\theta}\right) + \frac{d}{d\theta}\left(\frac{N_1}{R^2}\frac{dw}{d\theta}\right) - \frac{1}{R}N_1 = 0 \tag{2.40}$$

where the additional resultants about the equilibrium state are defined as

$$N_1 = A\varepsilon_1$$

$$M_1 = D\kappa_1 \tag{2.41}$$

The boundary conditions are

$$v_1(\pm\beta) = 0$$

$$w_1(\pm\beta) = 0$$

$$M_1(\pm\beta) = 0 \tag{2.42}$$

Equilibrium eq. (2.39) shows that the additional resultant is spatially uniform. Using the first of eqs. (2.41), eq. (2.35) and the boundary conditions on v_1 given by first of the eqs. (2.42), the additional thrust can be shown to be

$$N_1 = \frac{A}{2\beta}\int_{-\beta}^{+\beta}\left(\frac{1}{R}w_1 + \frac{1}{R^2}\frac{dw}{d\theta}\frac{dw_1}{d\theta}\right)d\theta \tag{2.43}$$

Now substitute eq. (2.37) into the second of the eqs. (2.41), and then substituting this result into eq. (2.40) yields the following ordinary differential equation for $w_1(\theta)$:

$$-\frac{D}{R^4}\frac{d^4 w_1}{d\theta^4} + \frac{N}{R^2}\frac{d^2 w_1}{d\theta^2} + N_1\left(\frac{1}{R^2}\frac{d^2 w}{d\theta^2} - \frac{1}{R}\right) = 0 \tag{2.44}$$

The boundary conditions for the additional normal displacements are

$$w_1(\pm\beta) = 0$$

$$\left.\frac{d^2 w_1}{d\theta^2}\right|_{\theta=\pm\beta} = 0 \tag{2.45}$$

Equations. (2.43)-(2.45) are satisfied by the trivial solution $w_1(\theta) = 0$ for $-\beta \le \theta \le \beta$. Nontrivial solutions for $w_1(\theta)$ occur for critical equilibrium states, which are manifest in eq. (2.43) and (2.44) through displacement $w(\theta)$ and resultant N.

In addition to the dimensionless variables defined by eqs. (2.20) and (2.25-2.27), the dimensionless additional displacement and additional resultant are defined as

$$\phi_1 = -\frac{w_1}{R\beta^2}$$

$$\eta_1 = -\frac{N_1}{A\beta^2} \tag{2.46}$$

Substituting these scaled variables and the ones defined previously into eqs. (2.43)-(2.45) yields

$$\frac{1}{\lambda^4}\frac{d^4\phi_1}{d\Gamma^4} + \eta\frac{d^2\phi_1}{d\Gamma^2} + \eta_1\left(1 + \frac{d^2\phi}{d\Gamma^2}\right) = 0 \tag{2.47}$$

$$\eta_1 = \frac{1}{2}\int_{-1}^{+1}\left(\phi_1 - \frac{d\phi_1}{d\Gamma}\frac{d\phi}{d\Gamma}\right)d\Gamma \tag{2.48}$$

$$\phi_1(\pm 1) = 0 \qquad \left.\frac{d^2\phi_1}{d\Gamma^2}\right|_{\Gamma=\pm 1} = 0 \tag{2.49}$$

Finally, the total potential energy Π given by the eqs. (2.28-30) can be written in terms of the dimensionless variables as

$$\overline{\Pi} = \lambda^4(-\eta + e_a)^2 + \frac{1}{2}\int_{-1}^{+1}\left(\frac{d^2\phi}{d\Gamma^2}\right)^2 d\Gamma - \lambda^4 p\phi(0) - 2\lambda^4 e_a(-\eta + e_a) + e_b \left.\frac{d\phi}{d\Gamma}\right|_{-1}^{+1} \quad (2.50)$$

where the dimensionless potential energy is defined by

$$\overline{\Pi} = \Pi \frac{R}{D\beta} \quad (2.51)$$

Also, the second variation of total potential energy in dimensionless form is

$$\delta^2\overline{\Pi} = \lambda^4\left[\eta_1^2 - \frac{1}{2}\eta\int_{-1}^{+1}\left(\frac{d\phi_1}{d\Gamma}\right)^2 d\Gamma\right] + \frac{1}{2}\int_{-1}^{+1}\left(\frac{d^2\phi_1}{d\Gamma^2}\right)^2 d\Gamma \quad (2.52)$$

2.4 Solutions to the equilibrium equations

Since the nondimensional circumferential resultant η is spatially uniform, the governing differential equation for $\phi(\Gamma)$, eq. (2.21), may be solved by methods for linear differential equations with constant coefficients. In the solution of eq. (2.21), it is convenient to introduce a nondimensional thrust parameter q, defined as

$$q^2 = \eta\lambda^4 \quad (2.53)$$

Mathematica[24] code is used to obtain and check the solutions presented in this section. The input statements and explanations are presented in appendix A.

2.4.1 Solution for $q \neq 0, q \neq \pi, q \neq \pi/2$

With the definition of thrust given by eq. (2.53), the solution to the eq. (2.21), subject to boundary conditions given by eq. (2.23) and transition conditions given by eq. (2.24), is a function of q. This is given as

$$\phi(\Gamma) = \frac{1}{2}\left(1-\Gamma^2\right) + \frac{1}{q^2}\left(1-e_b\right)\left[1 - Sec[q]Cos[q\Gamma]\right] +$$

$$\frac{p\lambda^4}{2q^2}\left[-1 + |\Gamma| - \frac{1}{q}Sin[q|\Gamma|] + \frac{1}{q}Tan[q]Cos[q\Gamma]\right] \tag{2.54}$$

Substituting this solution of $\phi(\Gamma)$ into the resultant-displacement relation eq. (2.22) and using eq. (2.53) yields

$$c_{11}p^2 + c_{12}pe_b + c_{22}e_b^2 + c_1 p + c_2 e_b + c_3 e_a + c_0 = 0 \tag{2.55}$$

where the coefficients in this expression are transcendental functions of the thrust parameter q. These coefficients are defined as

$$c_{11} = 3\lambda^{12}\left[2qSec^2[q] + qCos[2q]Sec^2[q] - 3Tan[q]\right] \tag{2.56}$$

$$c_{12} = 12\lambda^8 q\left[-2Sec[q] + Sec^2[q] + Cos[2q]Sec^2[q] + qSec[q]Tan[q]\right] \tag{2.57}$$

$$c_{22} = 6\lambda^4 q^2 Sec^2[q]\left[2q - Sin[2q]\right] \tag{2.58}$$

$$c_1 = 12\lambda^8 qSec[q]\left[2 - Sec[q] - Cos[2q]Sec[q] - qTan[q]\right] \tag{2.59}$$

$$c_2 = 12\lambda^4 q^2 Sec^2[q][-2q + Sin[2q]] \tag{2.60}$$

$$c_3 = -48\lambda^4 q^5 \tag{2.61}$$

$$c_0 = 48q^7 + 12\lambda^4 q^3 Sec^2[q] - 4\lambda^4 q^5 Sec^2[q] - 4\lambda^4 q^5 Cos[2q] Sec^2[q] -$$

$$6\lambda^4 q^2 Sec^2[q] Sin[2q] \tag{2.62}$$

Equation. (2.55) relates the thrust parameter q to the applied loads p, e_a and e_b in the equilibrium state for a given arch rise parameter λ as long as $q \neq 0$, $q \neq \pi/2$, $q \neq \pi$. Setting $e_a = e_b = 0$ in eqs. (2.54) and (2.55) reduces them to the solutions given by Carper[25].

2.4.2 Solution for $q = \pi/2$

In this case, the Fredholm alternative theorem applies to the solution of the boundary value problem given by eqs. (2.21), (2.23) and (2.24). The given boundary value problem cannot have a unique solution if the adjoint homogeneous boundary value problem has a solution other than identically zero. When the adjoint problem has a non-zero solution, the Fredholm theorem provides an orthogonality condition that must be satisfied for the existence of the solutions to eqs. (2.21), (2.23) and (2.24). To determine the adjoint problem, the inner product of eq. (2.21) with the (adjoint) function $\hat{\phi}(\Gamma)$ is formed and the result is integrated by parts using the boundary conditions of eqs. (2.23) and the transition conditions of eqs. (2.24). The adjoint homogeneous boundary value problem is

$$\frac{d^4}{d\Gamma^4}\left(\hat{\phi}\right) + q^2 \frac{d^2}{d\Gamma^2}\left(\hat{\phi}\right) = 0 \tag{2.63}$$

$$\hat{\phi}(\pm 1) = 0 \qquad \left.\frac{d^2}{d\Gamma^2}\left(\hat{\phi}\right)\right|_{\Gamma=\pm 1} = 0 \tag{2.64}$$

$$\hat{\phi}(\Gamma) \text{ and its first three derivatives are continuous at } \Gamma = 0 \tag{2.65}$$

This adjoint homogeneous boundary value problem has nontrivial solutions for q equal to odd multiples of $\pi/2$ and integer multiples of π. For $q = \pi/2$, the nontrivial solution to eqs. (2.63-2.65) is

$$\hat{\phi} = Cos\left[\frac{\pi}{2}\Gamma\right] \tag{2.66}$$

In this case, the eqs. (2.21), (2.23) and (2.24) can be solved only if the loads are orthogonal to eq. (2.66) in the sense that

$$e_b \left.\frac{d\hat{\phi}}{d\Gamma}\right|_{-1}^{+1} - p\lambda^4\hat{\phi}(0) + \int_{-1}^{+1} q^2\hat{\phi}d\Gamma = 0 \tag{2.67}$$

If this condition is satisfied, then the problem either has no solution or the solution is not unique. Substituting eq. (2.66) into eq. (2.67) with $q = \pi/2$ gives

$$e_b\pi + p\lambda^4 - \pi = 0 \tag{2.68}$$

When the condition in eq. (2.68) is satisfied, then the solutions to eqs. (2.21-2.23) for $q = \pi/2$ are

$$\phi(\Gamma) = a_3 Cos\left[\frac{\pi}{2}\Gamma\right] + \frac{1}{2}\left(1-\Gamma^2\right) + \frac{2}{\pi}\left(1-e_b\right)\left[-1+|\Gamma| + \frac{2}{\pi}\left(1 - Sin\left[\frac{\pi}{2}|\Gamma|\right]\right)\right] \tag{2.69}$$

where coefficient a_3 is not determined. However, if eq. (2.69) is substituted into the thrust-displacement relation , eq. (2.22), along with eq. (2.53) for $q = \pi/2$, it yields

$$\frac{\pi^5}{16}a_3^2 + \pi^2 a_3 e_b + (3\pi - 8)e_b^2 - \pi^2 a_3 - 2(3\pi - 8)e_b - \pi^3 e_a - 8 + 3\pi - \frac{\pi^3}{6} + \frac{\pi^5}{4\lambda^4} = 0 \quad (2.70)$$

Hence, for $q = \pi/2$, the loads p and e_b are related by eq. (2.68), and specifying load e_a in addition, determines the coefficient a_3 from eq. (2.70). Note that this eq. (2.70) is quadratic in a_3, so that there are, in general, two values of a_3 corresponding to two equilibrium configurations when $q = \pi/2$.

2.4.3 Solution for $q = \pi$

For $q = \pi$, the nontrivial solution to the adjoint problem (2.63 - 2.65) is $\hat{\phi} = Sin[\pi\Gamma]$. If this solution is substituted into the orthogonality condition of eq. (2.67), then it is identically satisfied. That is, there is no restriction on the values of p and e_b like the result of eq. (2.68). However, the solution to the differential equation (2.21) for $\phi(\Gamma)$ results in an asymmetric configuration in this case. The solution satisfying eq. (2.21) subject to boundary conditions in eqs. (2.23), transition conditions in eqs. (2.24), and using the definition of q in eq. (2.53), is

$$\phi(\Gamma) = \frac{1}{2}\left(1 - \Gamma^2\right) + \frac{1}{\pi^2}\left(1 + Cos[\pi\Gamma]\right) - \frac{\lambda^4 p}{2\pi^2}\left[1 - |\Gamma| + \frac{1}{\pi}Sin[\pi|\Gamma|]\right] + bSin[\pi\Gamma] \quad (2.71)$$

where the antisymmetric amplitude b is not determined. Substituting this solution, eq. (2.71), into the thrust-displacement relation of eq. (2.22) gives

$$9\lambda^8 p^2 + 48\lambda^4 p e_b + 12\pi^2 e_b^2 + 12\pi^6 b^2 - 48\lambda^4 p - 24\pi^2 e_b -$$

$$48\pi^4 e_a + 12\pi^2 - 8\pi^4 + 48\frac{\pi^6}{\lambda^4} = 0 \tag{2.72}$$

Equation. (2.72) relates the applied loads p, e_a and e_b to the amplitude b for $q = \pi$. Given the loads, note that eq. (2.72) determines two values of b, in general, corresponding to two asymmetric equilibrium configurations. Again, the solution is not unique.

2.5 Nontrivial solutions to the stability equations

The differential eq. (2.47) for the additional displacement $\phi_1(\Gamma)$ is solved using the equilibrium displacement $\phi(\Gamma)$ given by eq. (2.54); that is, it is solved using $\phi(\Gamma)$ when $q \neq 0$, $q \neq \pi/2$ and $q \neq \pi$. The differential eq. (2.47) can be solved by methods for differential equations with constant coefficients since η and η_1 are spatially uniform. Corresponding to the definition of the thrust parameter q in eq. (2.53), the thrust parameter due to the additional displacement is defined as

$$q_1^2 = \eta_1 \lambda^4 \tag{2.73}$$

Again, *Mathematica*[24] is used to obtain and check the solutions presented in this section. The input code is given in appendix B. The solution of the stability differential equations is divided into four steps. First the differential equation (2.47) is solved for the second derivative of $\phi_1(\Gamma)$ by superimposing the homogeneous solution and the particular solution. The particular solution satisfies the term containing the equilibrium displacement $\phi(\Gamma)$, and the method of variation of parameters is used to determine it. Continuity of the third and the second derivative of ϕ_1 at $\Gamma = 0$ is enforced. Second, this solution for the

second derivative of ϕ_1 is integrated twice and continuity of first derivative and the function ϕ_1 is satisfied at $\Gamma = 0$. The result is

$$\phi_1(\Gamma) = -k_1 \frac{Sin[q\Gamma]}{q^2} - k_2 \frac{Cos[q\Gamma]}{q^2} + k_3\Gamma + k_4 + q_1^2 g(\Gamma) \tag{2.74}$$

where k_1, k_2, k_3 and k_4 are arbitrary constants and the function originating from the particular solution is

$$g(\Gamma) = \frac{Sec[q]}{16q^5}\Big(-8\lambda^4 pqCos[q]|\Gamma| + 20qCos[q\Gamma] - 20e_b qCos[q\Gamma] -$$

$$4\lambda^4 pq|\Gamma|Cos(q - q|\Gamma|) + 8q^2\Gamma Sin[q\Gamma] - 8q^2 e_b \Gamma Sin[q\Gamma] +$$

$$\lambda^4 pSin[q + q|\Gamma|] - 11\lambda^4 pSin[q - q|\Gamma|]\Big) \tag{2.75}$$

Third, the displacement $\phi_1(\Gamma)$ is substituted into the thrust relation of eq. (2.48) along with the displacement $\phi(\Gamma)$ of the equilibrium state, eq. (2.54) to get

$$q_1^2 = a_2 k_2 + \lambda^4 k_4 + a_5 q_1^2 \tag{2.76}$$

where

$$a_2 = \lambda^4 Sec[q]\Big(\lambda^4 p - 4q^2 + 2e_b q^2 - 2\lambda^4 pCos[q] + \lambda^4 pCos[2q] -$$

$$2q^2 Cos[2q] + \lambda^4 pqSin[q] + qSin[2q] - e_b qSin[2q]\Big) / 4q^2 \tag{2.77}$$

and

$$a_5 = \frac{\lambda^4 Sec^2[q]}{64q^7}(-36\lambda^4 pq + 36e_b\lambda^4 pq + 13\lambda^8 p^2 q + 64q^3 - 88e_b q^3 + 24e_b^2 q^3 -$$

$$16\lambda^4 pq^3 + 71\lambda^4 pqCos[q] - 71e_b\lambda^4 pqCos[q] + 8\lambda^8 p^2 qCos[q] - 16\lambda^4 pq^3 Cos[q] -$$

$$36\lambda^4 pqCos[2q] + 36e_b\lambda^4 pqCos[2q] + 9\lambda^8 p^2 qCos[2q] + 48q^3 Cos[2q] -$$

$$56e_b q^3 Cos[2q] + 8e_b^2 q^3 Cos[2q] - 16\lambda^4 pq^3 Cos[2q] + \lambda^4 pqCos[3q] -$$

$$e_b\lambda^4 pqCos[3q] - \lambda^8 p^2 Sin[q] - 14\lambda^4 pq^2 Sin[q] + 16e_b\lambda^4 pq^2 Sin[q] -$$

$$13\lambda^8 p^2 Sin[2q] - 16q^2 Sin[2q] + 32e_b q^2 Sin[2q] - 16e_b^2 q^2 Sin[2q] -$$

$$8\lambda^4 pq^2 Sin[2q] + 8e_b\lambda^4 pq^2 Sin[2q] + 16q^4 Sin[2q] -$$

$$16e_b q^4 Sin[2q] - \lambda^8 p^2 Sin[3q] + 2\lambda^4 pq^2 Sin[3q]) \tag{2.78}$$

Fourth, the solution for $\phi_1(\Gamma)$ in eq. (2.74) is substituted into the homogeneous boundary conditions given by eqs. (2.49), and eq. (2.76) is appended to these boundary equations, to get

$$\begin{bmatrix} \frac{Sin[q]}{q^2} & -\frac{Cos[q]}{q^2} & -1 & 1 & g(-1) \\ -Sin[q] & Cos[q] & 0 & 0 & g''(-1) \\ -\frac{Sin[q]}{q^2} & -\frac{Cos[q]}{q^2} & 1 & 1 & g(1) \\ Sin[q] & Cos[q] & 0 & 0 & g''(1) \\ 0 & a_2 & 0 & \lambda^4 & a_5 - 1 \end{bmatrix} \begin{bmatrix} k_1 \\ k_2 \\ k_3 \\ k_4 \\ q_1^2 \end{bmatrix} = 0 \tag{2.79}$$

where g'' denotes the second derivative of function g with respect to Γ. This 5 x 5 matrix equation (2.79) is equivalent to a 2 x 2 matrix equation for the antisymmetric solution and a 3 x 3 matrix equation for the symmetric solution. Note that the function $g(\Gamma)$ is symmetric so that $g(-1) = g(1)$ and $g''(-1) = g''(1)$. The antisymmetric solution is obtained from eq. (2.79) by subtracting row three from row one and subtracting row four from row two to get

$$\begin{bmatrix} \frac{Sin[q]}{1} & -1 \\ -Sin[q] & 0 \end{bmatrix} \begin{bmatrix} k_1 \\ k_3 \end{bmatrix} = 0 \tag{2.80}$$

Non-trivial solutions to eq. (2.80) occur for q equal to integer values of π and $k_3 = 0$. (also, $k_2 = k_4 = q_1^2 = 0$.) Thus, the lowest antisymmetric buckling mode is

$$\phi_1(\Gamma) = -\frac{k_1}{q^2} Sin[q\Gamma] \qquad \text{and} \qquad q = \pi \tag{2.81}$$

with amplitude k_1 undetermined. Equation (2.81) corresponds to a critical equilibrium state at a bifurcation point on the primary (symmetric) equilibrium path. That is, the antisymmetric buckling mode of eq. (2.81) is obtained by considering a perturbation about the symmetric equilibrium state given by eq. (2.54). The load p, e_a and e_b in this critical equilibrium state corresponding to $q = \pi$ are related by eq. (2.72) with the asymmetric amplitude $b = 0$.

A critical equilibrium state defined by a symmetric buckling mode (a limit point) is determined from the manipulation of eq. (2.79) in the following manner : add rows one and three, add rows two and four and repeat the non-zero elements of row five to get

$$\begin{bmatrix} -\frac{Cos[q]}{q^2} & 1 & g(-1) \\ Cos[q] & 0 & g''(-1) \\ a_2 & \lambda^4 & a_5 - 1 \end{bmatrix} \begin{bmatrix} k_2 \\ k_4 \\ q_1^2 \end{bmatrix} = 0 \tag{2.82}$$

A non-trivial solution for k_2, k_4 and q_1^2 requires the determinant of coefficients in eq. (2.82) to vanish. Vanishing of this determinant gives the stability equation for symmetric buckling in the form

$$\begin{aligned} & s_{20}p^2 + s_{11}pe_b + s_{02}e_b^2 + \\ & s_{10}p + s_{01}e_b + \\ & s_{00} = f = 0 \end{aligned} \tag{2.83}$$

where coefficients s_{ij}, i, j = 0,1,2 are transcendental functions of q and also depend on λ. These coefficients are

$$s_{20} = \left(-\frac{\lambda^{12}Sec^2[q]}{128q^7}\right)\left(52qCos[q] + 8qCos[3q] - 15Sin[q] - 8q^2Sin[q] - 15Sin[q]\right) \tag{2.84}$$

$$\begin{aligned} s_{11} = \left(\frac{\lambda^8 Sec^2[q]}{16q^6}\right)\Big(8 + 3q^2 - 12Cos[q] + 8Cos[2q] - \\ q^2Cos[2q] - 4Cos[3q] - 5qSin[2q]\Big) \end{aligned} \tag{2.85}$$

$$s_{02} = \left(\frac{\lambda^4 Sec^2[q]}{32q^5}\right)\left(-12qCos[q] + 3Sin[q] + 8q^2Sin[q] + 3Sin[3q]\right) \tag{2.86}$$

$$s_{10} = \left(\frac{\lambda^8 Sec^2[q]}{16q^6}\right)\left(-8 - 3q^2 + 12Cos[q] - 8Cos[2q] + \right.$$

$$\left. q^2 Cos[2q] + 4Cos[3q] + 5qSin[2q]\right) \tag{2.85}$$

$$s_{01} = \left(\frac{\lambda^4 Sec^2[q]}{16q^5}\right)\left(12qCos[q] - 3Sin[q] - 8q^2 Sin[q] - 3Sin[3q]\right) \tag{2.86}$$

$$s_{00} = \left(\frac{Sec^2[q]}{32q^5}\right)\left(-12\lambda^4 qCos[q] + 24q^5 Cos[q] + 8q^5 Cos[3q] + \right.$$

$$\left. 3\lambda^4 Sin[q] + 8\lambda^4 q^2 Sin[q] + 3\lambda^4 Sin[3q]\right) \tag{2.87}$$

Equation (2.83) is used in the sequel to evaluate if a symmetric equilibrium state, eq. (2.54) is critical in a symmetric buckling mode. That is, f is evaluated from eq. (2.83) for a symmetric equilibrium configuration, eq. (2.54), to determine if it is critical or not. In practice, it is known that the equilibrium states emanating from the origin in the load space are stable and moving away from the origin along some path in the load space results in critical equilibrium to occur for $f = 0$. In this sense, it can be determined if a critical point occurs on the load path, which indicates a change in the stability of the equilibrium states along the path.

3. *Induced Strain Path Selection In Load Space*

The manner in which the induced strains Λ_b and Λ_t are prescribed is presented in this chapter. The approach developed is best described in a three dimensional load space spanned by three Cartesian coordinate axes identified as Λ_b, Λ_t and the midspan load p. Then the objective is to determine a path in a p = constant plane of the load space such that the arch displaces through a set of stable equilibrium states to an inverted configuration. The first section of this chapter reviews the equilibrium response of the arch without induced strain actuation, and subsequent sections build on these results to describe the strategy for prescribing the induced strains.

3.1 Equilibrium states for $\lambda = 2.10$, $\Lambda_b = \Lambda_t = 0$

For $\lambda = 2.10$ and induced strains $\Lambda_b = \Lambda_t = 0$, the arch exhibits the limit point behavior under the midspan load p. This particular value of the arch rise parameter λ is selected to illustrate limit point behavior quantitatively. Limit point behavior is exhibited by a pin-ended, shallow circular arch under midspan load for $1.976 < \lambda < 2.825$.

For $\lambda = 2.10$ and the scaled actuation strain parameters $e_a = e_b = 0$ (see eqs. 2.26), the equilibrium states are obtained by specifying the thrust parameter q in eqs. (2.56 - 2.62), and then solving the resulting quadratic equation (2.55) for roots p. If the physically impossible case of complex roots occurs, then the value of q is too large and smaller value must be selected. In general, two real roots for p are determined for each value of q. Each root corresponds to a different equilibrium state having the same value of the thrust parameter. (Recall eq. (2.55) is valid if $q \neq 0, q \neq \pi / 2, q = \pi, etc$. If the solutions for $q = \pi/2$ and $q = \pi$ are required then the solutions given in Sections 2.4.2 and 2.4.3, respectively, are used instead of eq. (2.55). However, it turns out that when $q = \pi$ for $\lambda = 2.10$, imaginary values of p result which is a physically meaningless case). For each combination of q and p, the dimensionless center displacement is computed. The center displacement is determined from eq. (2.54) to be

$$\phi(0) = \frac{1}{2} + \frac{1}{q^2}(1 - Sec[q]) + \frac{p\lambda^4}{2q^2}\left(-1 + \frac{1}{q}Tan[q]\right) \tag{3.1}$$

With equilibrium values of p, q and $\phi(0)$ known, we plot the equilibrium states on the load-thrust plane (p *vs.* q) and the load-displacement plane (p *vs.* $\phi(0)$). The results for p

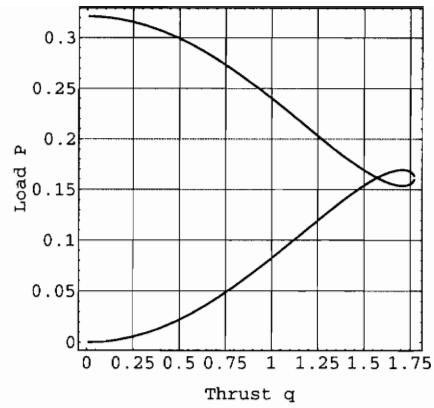

(a) Load-thrust (p-q) plot

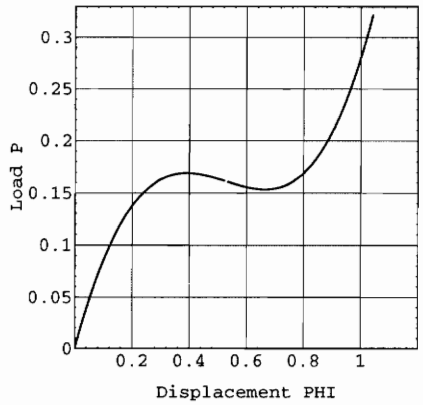

(b) Load-displacement (p-PHI) plot

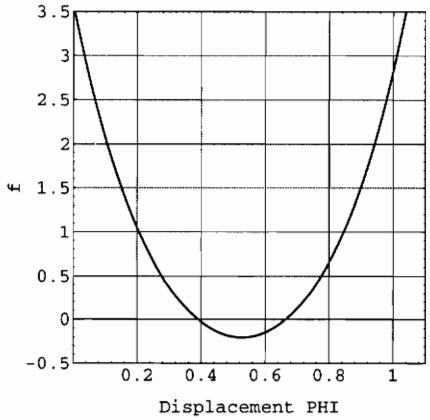

(c) Stability function f

Figure 3.1 Equilibrium states and stability function, *f*, for an arch with $\lambda = 2.10$ and no actuation strains.

vs. q and p *vs.* $\phi(0)$ are shown in Figure 3.1(a) and 3.1(b). In addition, the value of f is computed from the stability equation (2.83) for each equilibrium state. The values of f are plotted versus the midspan displacement in Figure 3.1(c).

Critical equilibrium states occur when the value of the stability equation is zero. As can be seen in Figures 3.1(b) and 3.1(c), critical states occur at the limit points on the load-displacement plot. If the stability of the equilibrium states change along the equilibrium path, then the change occurs at the critical points. The arch is stable at no load and remains stable as the load is increased to the upper limit point. The stability function, f, is positive for these stable states as shown in Figure 3.1(c). The equilibrium path is unstable between the upper and lower limit points. Note that the function f goes through zero at the upper limit point and the lower limit point and is negative between them. The equilibrium states are stable after the lower limit point. Again function f is positive after the lower limit point.

Strictly speaking, the sign of function f is not sufficient to indicate stability or instability. The criterion for stability is that the second variation of the total potential energy, see eqs(2.34) and (2.52), is positive definite for every kinematically admissible displacement ϕ_1 about the equilibrium state. Function $f = 0$ merely indicates the critical equilibrium states.

All the results presented in this work are for $\lambda = 2.10$, where the instability can only occur by buckling in a symmetric mode; e.g., at limit points when $e_a = e_b = 0$, The arch cannot be unstable in an antisymmetric buckling mode since the thrust parameter $q < \pi$ for all symmetric equilibrium states.(Refer to eqs. (2.80) and (2.81).) For this small value of l, then, we assume any instability occurs in a single symmetric buckling mode, and that the stability of the equilibrium states can be inferred from the sign of f.

3.2 The preferred equilibrium path

The specific load - displacement and the load - thrust plots of the previous section are explained in a qualitative way for limit point behavior using Figure 3.2. As the load increases from point 0 to point 1, thrust increases while stiffness tends to decrease. At point 2, which is the upper limit point, the arch is in a critical state of equilibrium. Increasing the load beyond this relative maximum value will cause the arch to dynamically snap through from its position at point 2 to that at point 6. On the portion 2-3-4 of the equilibrium path, thrust continues to increase till it reaches a maximum at point 3. Beyond this point, the thrust tends to decrease with the load till the load reaches a relative minimum at point 4 (lower limit point). On portion 4-5-6-7 of the equilibrium path, thrust continues to decrease. In Figure 3.2, the portions 0-1-2 and 4-5-6-7 are stable while the descending portion 2-3-4 is unstable. To avoid a drop in the load along the portion 2-3-4-5-6 of the equilibrium path, an alternative path from point 2 to 6 is preferred. This alternative path connecting points 2 and 6 is shown as a dashed line in Figure 3.2. On path 2-6, the midspan load p remains constant.

In order to move along this alternative path 2--6, an external force apart from the midspan load p is required to guide the arch through. This external force is provided by the PZT actuation loads e_a and e_b. Thus, a suitable distribution of e_a and e_b is required over the path 2-6.

3.3 Method of selecting actuation strains

The procedure to find the actuation strains along the alternative equilibrium path 2-6 of Figure 3.2 is based on a plot of midspan displacement versus the thrust. For the case of non-zero actuation strains, the midspan displacement is determined from eq. (2.54) to be

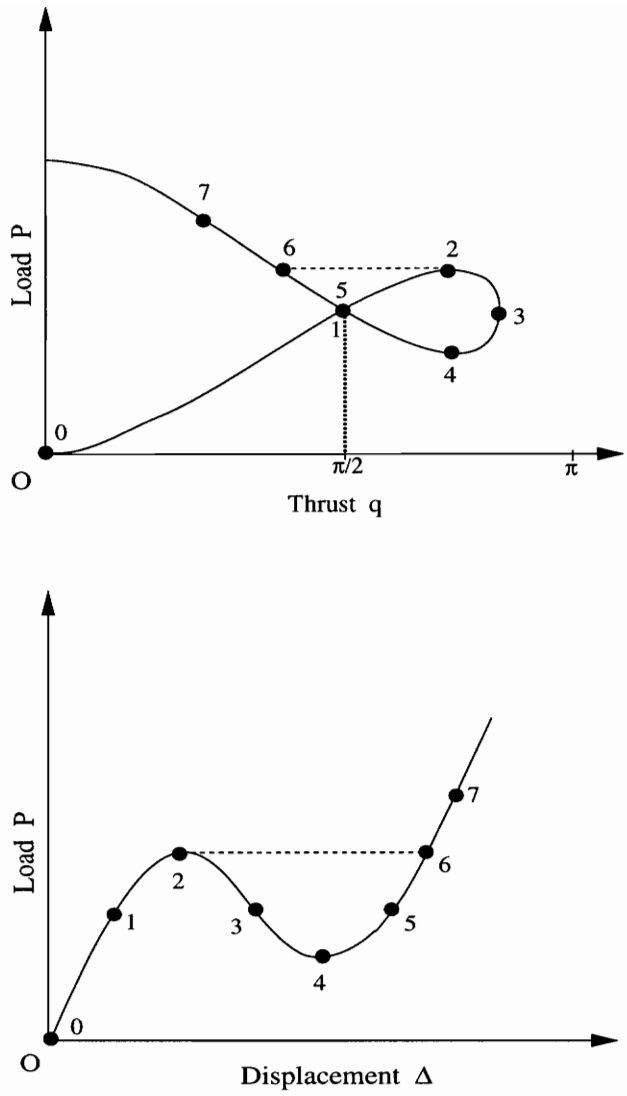

Figure 3.2 Load-thrust(p-q) and load-displacement (p-Δ) diagrams for a shallow arch

$$\phi(0) = \frac{1}{2} + \frac{1}{q^2}(1 - e_b)(1 - Sec[q]) + \frac{p\lambda^4}{2q^2}\left(-1 + \frac{1}{q}Tan[q]\right) \tag{3.2}$$

On path 2-6, the load p is a prescribed constant. At the end points 2 and 6, $e_a = e_b = 0$ and the values of q and $\phi(0)$ are known. These end point values satisfy eq. (3.2) identically. The procedure to find e_a and e_b between the end points is as follows:

a) Select a path between points 2 and 6 in the displacement - thrust plane shown in Figure 3.3.

b) From the path selected in (a), determine a value for e_b from eq. (3.2) for each value of q and $\phi(0)$.

c). From the equilibrium - thrust relation, eq. (2.55), calculate a value for e_a for each value of q, $\phi(0)$, and e_b.

d) Compute the value of the stability equation, eq. (2.83), for values of p, e_a, e_b and q of the equilibrium state on path 2-6.

Several possible paths from point 2 to point 6 in the displacement - thrust plane are shown in Figure 3.3. Numerical results for these paths are presented in the next chapter.

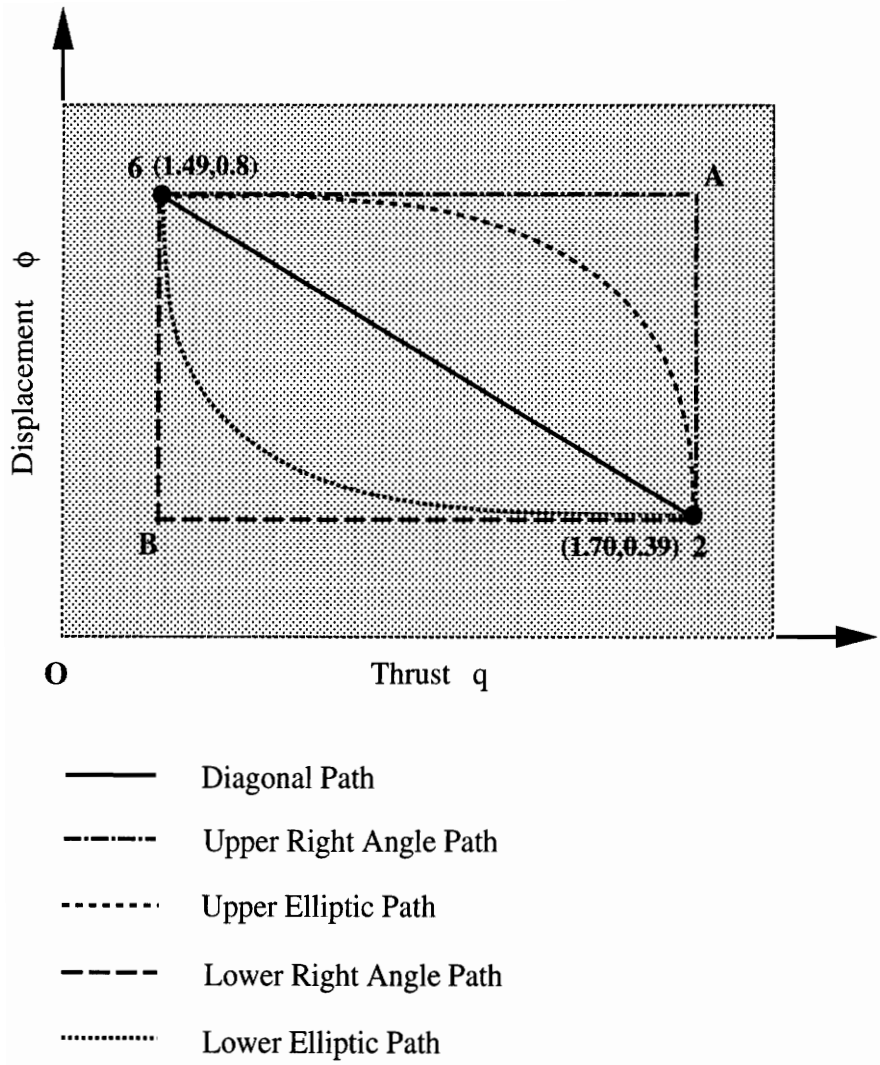

Figure 3.3. Paths selected in q-ϕ plane

4. Numerical Results

The structural response problem is normally posed as:determine the equilibrium configurations given the loads. In chapter 3 the inverse problem is formulated. That is, equilibrium paths are selected that displace the arch to an inverted configuration at a constant value of the midspan load, and then the actuation load parameters e_a and e_b are determined. The numerical results for this inverse formulation are presented in this chapter using a fixed value of 2.10 for the arch rise parameter λ. As mentioned earlier, limit point behavior is exhibited by pin-ended, shallow, circular arch under a midspan load and no actuation loads for $1.976 < \lambda < 2.825$. A low value of $\lambda = 2.10$ is selected in order to keep the magnitude of the actuation strains low. Actuation loads e_a and e_b are evaluated for the equilibrium paths shown in Figure 4.1, which is repeated from Chapter 3. The stability

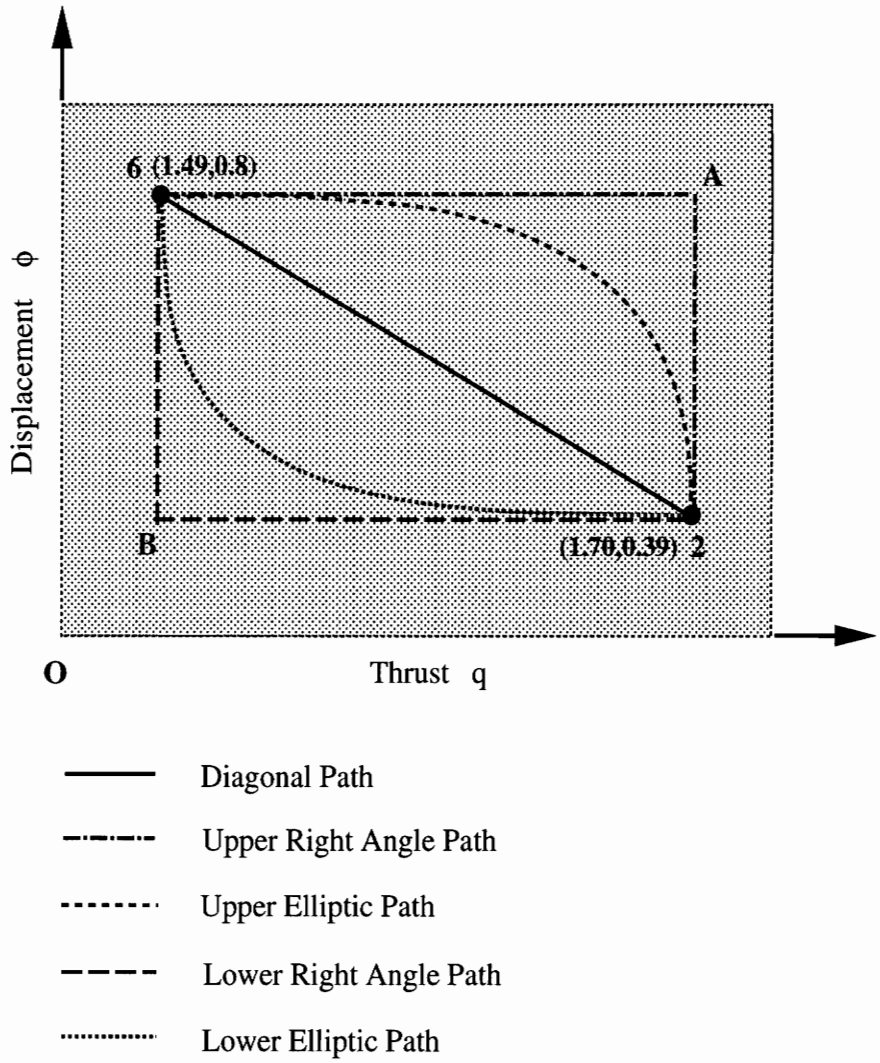

Figure 4.1 Equilibrium paths selected in q-ϕ plane for $\lambda = 2.10$ and $p = 0.169312$.

function f of is evaluated for each of these paths. This is followed by a more detailed analysis of the lower elliptic path for a specific geometry and materials. Then circumferential normal strain and stress distributions through the thickness at midspan for the selected equilibrium states are presented. These strain and stress results help quantify the load redistribution due to induced strains Λ_b and Λ_t.

4.1 A measure of total load

Consider a three dimensional load space spanned by three Cartesian coordinates axes e_a, e_b, and midspan load p, and some load path as shown in Figure 4.2. Then, the measure of the total load is the magnitude of the ray from the origin to a point on the load path. The total

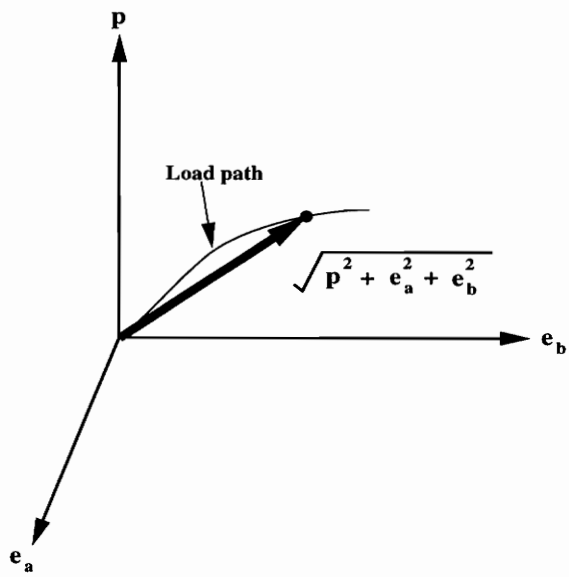

Figure 4.2 Total load measure in the three dimensional load space

load at each point on the load path is, then, the square root of the sum of the squares of the loads e_a, e_b and p. Based on the considerations presented in chapter 3, actuator loads e_a and e_b contribute to the total load only along the alternate path, i.e., $e_a \neq 0$ and $e_b \neq 0$ for $0.39 < \phi(0) < 0.80$.

4.2 Results for alternate equilibrium paths

4.2.1 Diagonal path

This was the first path selected and analyzed. This path is a straight line joining point 2 and point 6 (Figure 4.1). Moving along this path from point 2 to point 6 reduces thrust at a constant rate while increasing the midspan displacement. The e_a and e_b distributions are obtained as outlined in Chapter 3. These distributions are used to evaluate the stability function, f, and the total load along the equilibrium path.

The e_a and e_b distributions for the diagonal path are shown in Figure 4.3a. The points 2 and 6 coincide on the e_a-e_b plane since the values of the actuation loads at these points are both zero. The total load is plotted against the midspan displacement in Figure 4.3b. The value of f from the stability equation (2.83) is computed for each equilibrium state and plotted against the midspan displacement, $\phi(0)$, in Figure 4.3c. The points at which $f = 0$ denote the critical equilibrium states. The critical equilibrium states occur for $\phi(0) = 0.39$ and $\phi(0) = 0.67$ for an arch without actuation. (Refer to Figure 3.1c). For the actuation strain distribution obtained along the diagonal path, the critical equilibrium states occur for $\phi(0) = 0.39$ and $\phi(0) \approx 0.6$. This implies that on the diagonal path, the equilibrium states are unstable for $0.39 < \phi(0) < 0.6$. Thus, the actuation strain distributions obtained from the diagonal path are unable to provide a stable alternate equilibrium path. These actuation

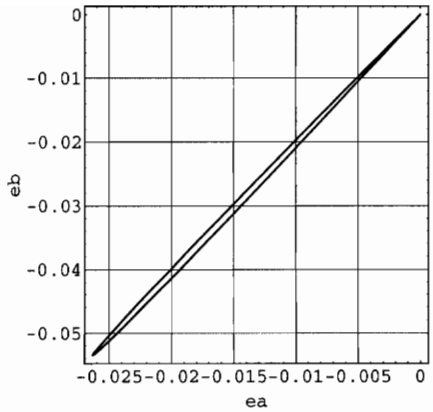

(a) Actuation load distribution

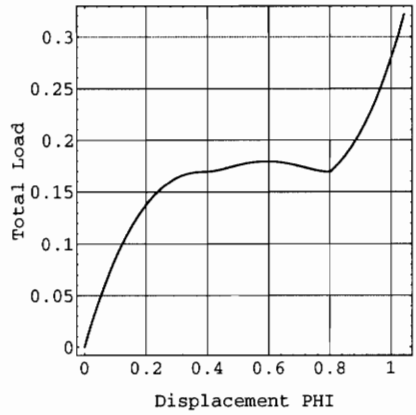

(b) Total load vs. midspan displacement

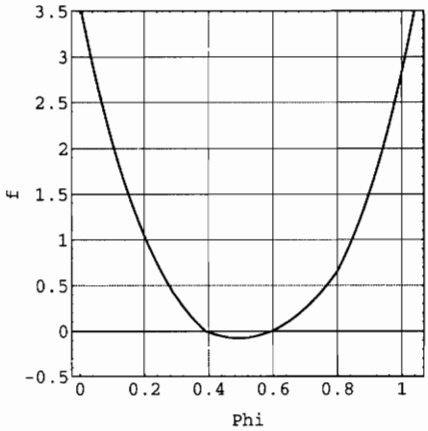

(c) Stability function f along the equilibrium path

Figure 4.3 Diagonal path results for $\lambda = 2.10$.

strain distributions are, however, successful in reducing the length of the unstable portion of the equilibrium path 2-6.

4.2.2 Upper right angle path

The upper right angle path (see Figure 4.1) is a bilinear path. Along the first segment, 2-A, of this path, thrust q is held constant at its value at point 2. The midspan displacement is allowed to increase from $\phi(0) = 0.39$, its value at point 2, to $\phi(0) = 0.80$, its value at point 6. Along the second segment, A-6, of this path, the midspan displacement is held constant at $\phi(0) = 0.80$ and the thrust q is allowed to decrease to its value $q = 1.49$ at point 6.

The e_a and e_b distributions for this path are shown in Figure 4.4a and the total load along this path is shown in Figure 4.4b. The value f of the stability equation is plotted against the midspan displacement in Figure 4.4c. The critical equilibrium states on this path occur at $\phi(0) = 0.39$ and $\phi(0) \approx 0.67$. This implies that the equilibrium path is unstable for $0.39 < \phi(0) < 0.67$. Therefore, the upper rectangular path is unable to provide a suitable actuation strain distribution to produce a stable equilibrium path

4.2.3 Lower right angle path

The lower right angle path is also a bilinear path like the upper right angle path. However, unlike the upper right angle path, in the lower right angle path the thrust q is first reduced holding the midspan displacement constant. Thus, over the first segment, 2-B, of this path, thrust is reduced to $q = 1.49$, its value at point 6 while holding the displacement constant at $\phi(0) = 0.39$. Then along the second segment, B-6, the midspan displacement is allowed to increase to $\phi(0)= 0.80$, its value at point 6, keeping the thrust constant at $q = 1.49$. Thus, the lower right angle path first reduces the thrust while holding the midspan

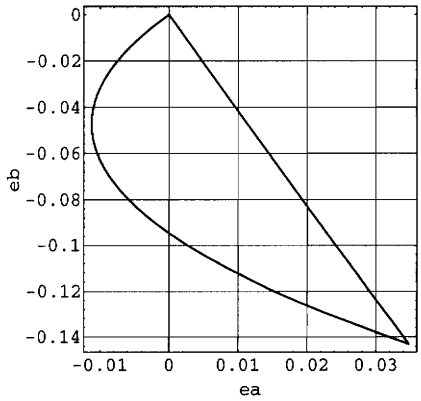

(a) Actuation load distribution

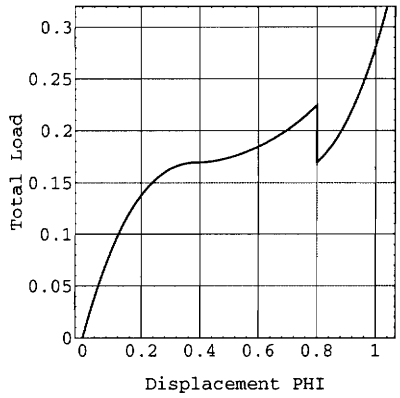

(b) Total load vs. midspan displacement

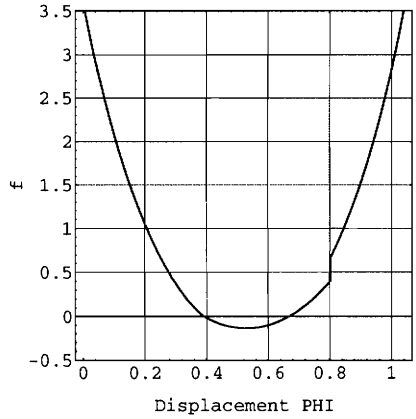

(c) Stability function f along the equilibrium path

Figure 4.4 Upper right angle path results for $\lambda = 2.10$.

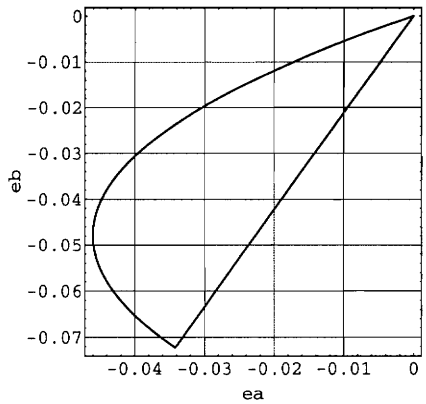

(a) Actuation load distribution

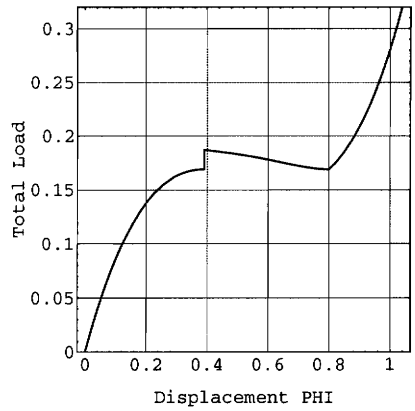

(b) Total load vs. midspan displacement

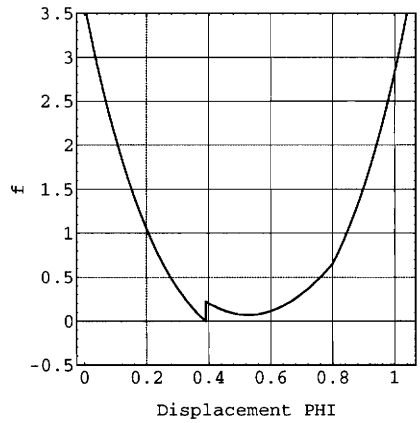

(c) Stability function f along the equilibrium path

Figure 4.5 Lower right angle path results for $\lambda = 2.10$.

displacement constant and then at that reduced value of the thrust, allows the midspan displacement to increase to its value at point 6.

The e_a vs. e_b plot for this path is shown in Figure 4.5a. The total load is for this path is plotted in Figure 4.5b and the value of the stability equation, f, for this path is shown in Figure 4.5c. The critical equilibrium state occurs only at the midspan displacement $\phi(0) = 0.39$. The value of f is positive for $0.39 < \phi(0) < 0.80$ on this path. The implication is that the equilibrium path is stable at all points along the lower right angle path except at point 2 at which it is critical. Thus, the actuation strain distribution along the lower right angle path appears to successfully provide a stable equilibrium path except, perhaps, at point 2.

4.2.4 Lower elliptic path

The lower elliptic path is a segment of an ellipse with its center at $q = 1.70$ and $\phi(0) = 0.80$. See Figure 4.1. The lower elliptic path is selected because of its resemblance to the lower right angle path in first reducing the thrust before any large increase in midspan displacement is made.

The e_a vs. e_b plot for the elliptic path is shown in Figure 4.6a, and the total load and the stability function f are plotted in Figure 4.6b and Figure 4.6c, respectively. The value of $f = 0$ at $\phi(0) = 0.39$ only. This is shown in Figure 4.6d which is an enlarged view of the middle section of the Figure 4.6c. The value of f is positive at all the other points on the lower elliptic path. Therefore, this path is apparently stable at all the points except, perhaps, at $\phi(0) = 0.39$. Thus, the lower elliptic path appears to successfully generate an e_a and an e_b distribution which is capable of providing a stable equilibrium path. The e_a and e_b distribution obtained is also lower in magnitude than the those obtained from the lower

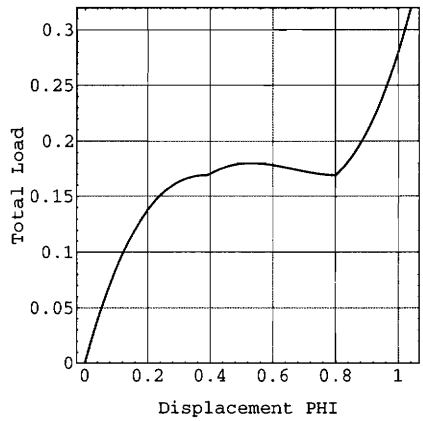

(a) Total load vs. midspan displacement

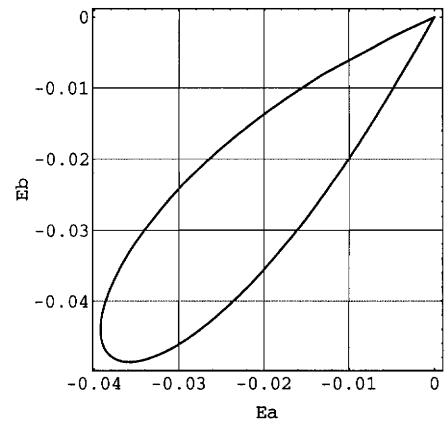

(b) Actuation load distribution

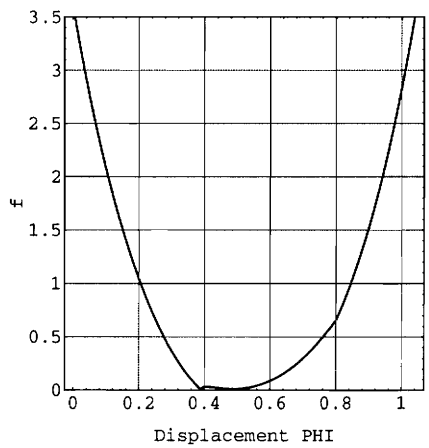

(c) Stability function f along equilibrium path

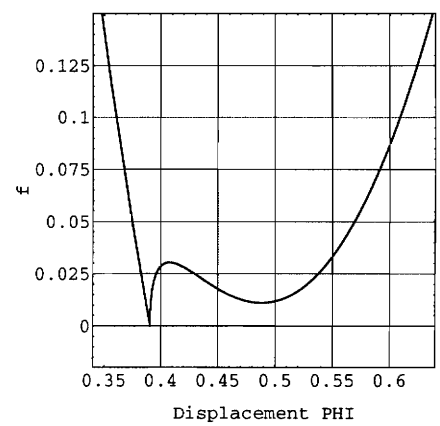

(d) A blow-up of Figure (c)

Figure 4.6 Lower elliptic path results for $\lambda = 2.10$.

right angle path. This path is, therefore, preferred to the lower right angle path.

4.3 Elliptic load path and a baseline configuration

Of all the paths that have been analyzed, the lower elliptic path appears to be the most suitable. It appears to provide a stable equilibrium path and also the lowest actuation loads among all the paths that were studied. It may also be noticed that the stable equilibrium path was obtained for all the paths in which initially the thrust was reduced at a rate greater than the rate at which the midspan displacement was allowed to increase.

4.3.1 Actuation strains Λ_b and Λ_t

The actuation load parameters e_a and e_b are used to calculate the induced actuation strains using eqs. (2.26). The baseline geometric and material properties for the arch that are used for evaluating the actuation strains are given in Table 4.1. The actuation strain distribution for the elliptic path is shown in Figure 4.7a. These actuation strains are interpreted in terms of the voltages, V_b and V_t (eq. (1.17)), and are plotted in Figure 4.7b. Note that both actuation strains are negative.

Table 4.1. Baseline geometric parameters and material properties used for evaluating actuation strains Λ_b and Λ_t for $\lambda = 2.10$.

Parameters	Value
Arch radius R	25.0 in.
Semi-opening angle β	2.89 deg.
Arch parameter, λ	2.10
Total arch thickness, h	0.05 in.

Elastic modulus for PZT, E_a	1 x 10^7 psi
Elastic modulus for core E_2	1 x 10^7 psi
Poisson's ratio for PZT, v_a	0.30
Poisson's ratio for core, v_2	0.30
Piezoelectric strain coefficient, d_{31}	-6.732 x 10^{-09} inches/Volt
Polarization field	50,800 Volts/inches
Initial depolarization field	12,700 Volts/inches
PZT thickness, t_1	0.01 inches

4.3.2 Stress and strain distribution

The stress and strain distributions through the thickness at the midspan are computed for selected equilibrium states and for the data given in Table 4.1. First the middle surface strain ε is calculated from the first constitutive law in eqs. (2.14), then the change in curvature κ is computed from eq. (2.3), and finally with these results, the circumferential normal strain is computed from the second of eqs. (2.2). The circumferential normal stress is computed from eqs. (2.13).

The selected equilibrium states are shown in Figure 4.8 and quantified in Table 4.2. The comparison of stresses and strains between equilibrium state S_1 (actuators active) and state S_2 (actuators not active) are shown in Figure 4.9. These two equilibrium states have the same thrust but different load and midspan displacement as indicated in Table 4.2. The induced strain actuators reduce the bending strain magnitude and increase the compressive membrane strain slightly. Bending stresses are reduced in the piezoelectric layers with the actuators active.

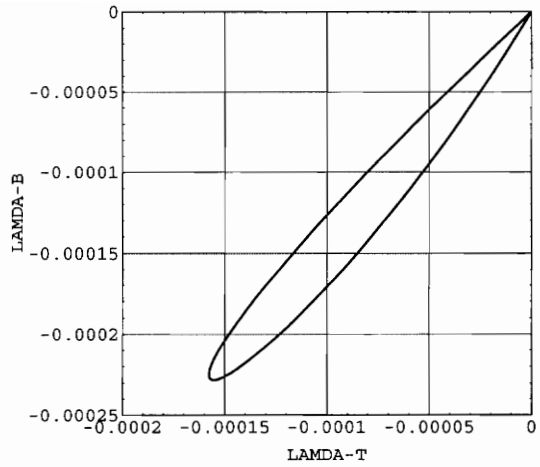

(a) Actuation strains in the top and bottom PZT layers

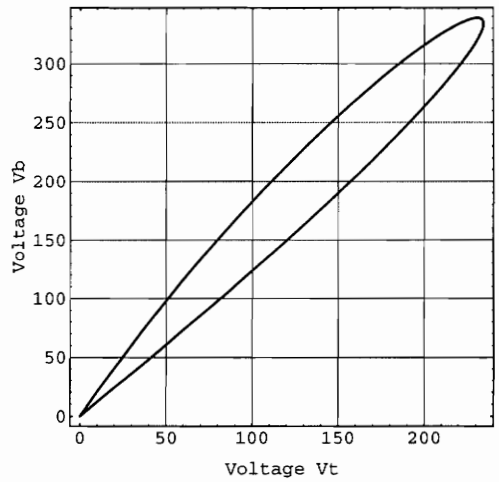

(b) Voltage distribution in the top and bottom PZT layers

Figure 4.7 Actuation strain distribution and voltage distribution for the lower elliptic path, $\lambda = 2.10$, and the baseline date given in Table 4.1.

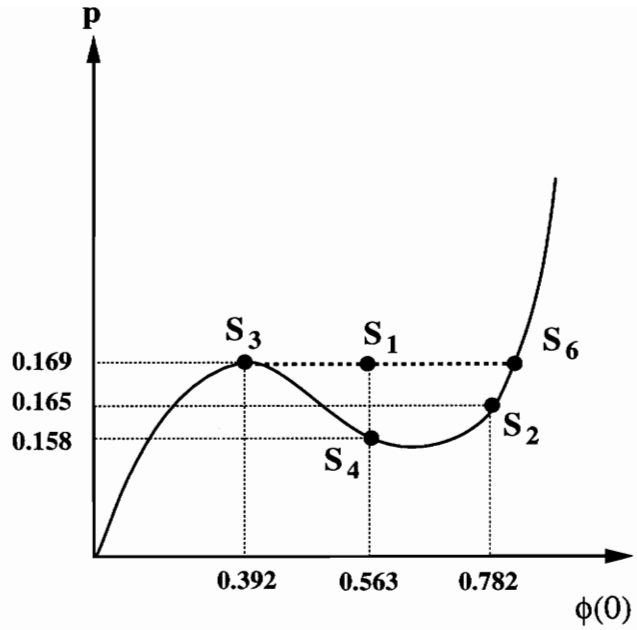

Figure 4.8 Selected equilibrium states on the p-$\phi(0)$ plane for $\lambda = 2.10$ including the lower elliptic alternative path.

Table 4.2 Values of loads, thrust and midspan displacement for selected equilibrium states

State	p	e_b	e_a	q	$\phi(0)$
S_1	0.16931	-0.04431	-0.039247	1.53611	0.56389
S_2	0.16503	0.0	0.0	1.53611	0.78279
S_3	0.16931	0.0	0.0	1.49798	0.39058
S_4	0.15849	0.0	0.0	1.76774	0.56389
S_6	0.16931	0.0	0.0	1.49798	0.80102

The comparison of the stresses and strains between equilibrium state S_1 (actuators active) and state S_3 (actuators not active) are shown in Figure 4.10. These two equilibrium states have the same value of the midspan load (Table 4.2). The comparison again shows decreased bending strain when the actuators are active, and a small increase in the compressive membrane strain.

Lastly, the comparison between equilibrium states S_1 and S_4 (actuators not active) is shown in Figure 4.11. Each equilibrium state has the same midspan displacement. The strain distributions for state S_1 and S_4 are nearly identical as shown in Figure 4.11b.

These comparisons between equilibrium state S_1 (actuators active) and states S_2, S_3 and S_4 (actuators not active) indicate a decrease in bending strain with the actuators active. As a result of decreased bending strain, the total stress in the piezoelectric layers decreases relative to comparable equilibrium states with actuators not active (see Figures 4.9 and 4.10).

4.3.3 Mode shapes and the effect of induced loads

The configuration of the arch at specific equilibrium states S_1, S_3 and S_6 (see Figure 4.8 and Table 4.2) are shown in Figure 4.12. The dashed line represents the undeformed arch shape. The moment, M, at $\theta = \beta$ and the thrust, $-N$, are plotted along the alternate path in Figure 4.13a and 4.13b respectively. The total moment at $\theta = \pm\beta$ vanishes, so the mechanical portion and the induced portions add to zero. (Refer to constitutive eqs. (2.14).) In effect, the induced moment from the actuation strains is equivalent to a positive mechanical moment acting at the ends of the arch. A positive moment resists the downward displacement.

As shown in Figure 4.13(b), the thrust is decreased by the actuator strains : i.e., the

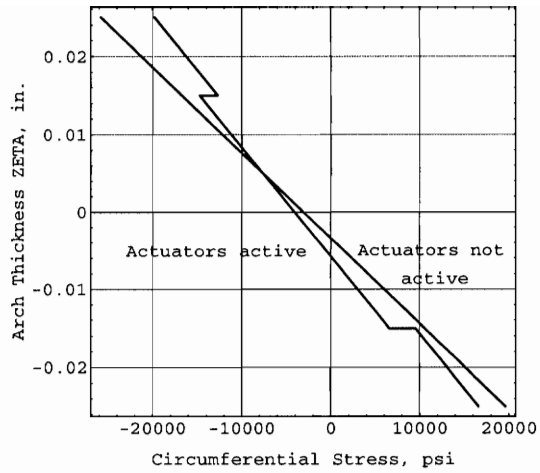

(a) Circumferential stresses in the arch with and without the actuators

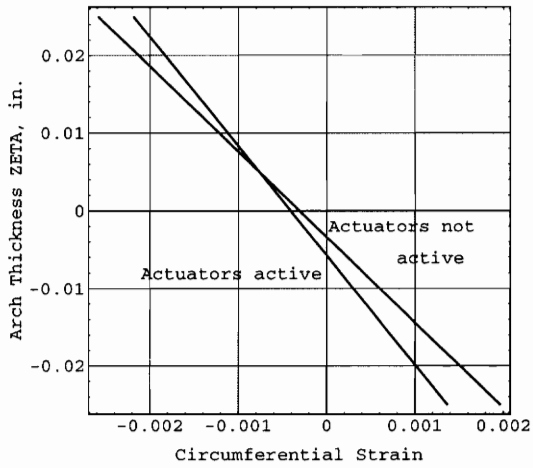

(b) Circumferential strains in the arch with and without the actuators

Figure 4.9 Circumferential stress and strain distribution through the thickness of the arch for equilibrium state S_1 (actuators active) and state S_2 (actuators not active), where each state has the same value of thrust.

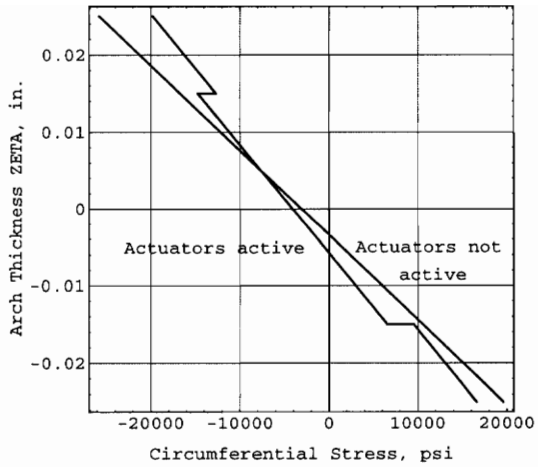

(a) Circumferential stresses in the arch with and without the actuators

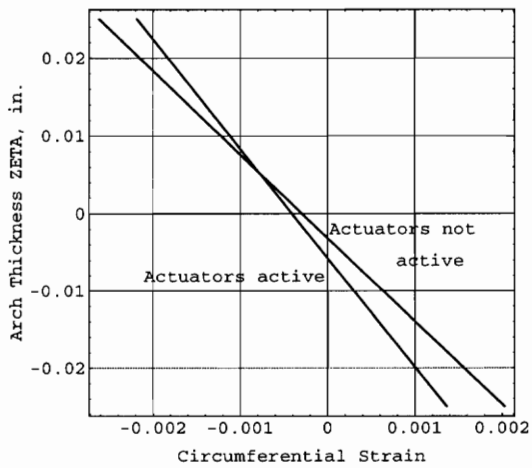

(b) Circumferential strains in the arch with and without the actuators

Figure 4.10 Circumferential stress and strain distribution through the thickness of the arch for equilibrium state S_1 (actuators active) and state S_3 (actuators not active), where each state has the same midspan load.

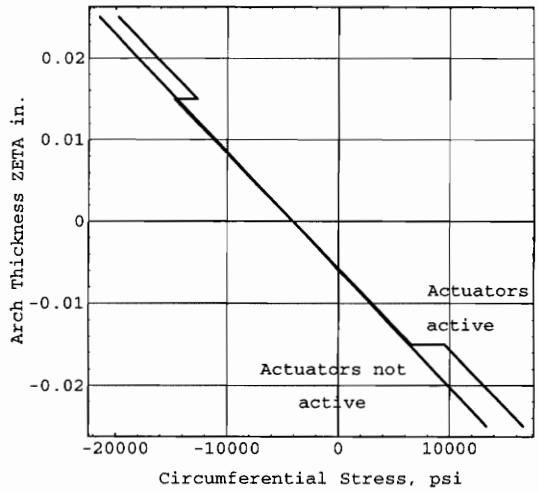

(a) Circumferential stresses in the arch with and without the actuators

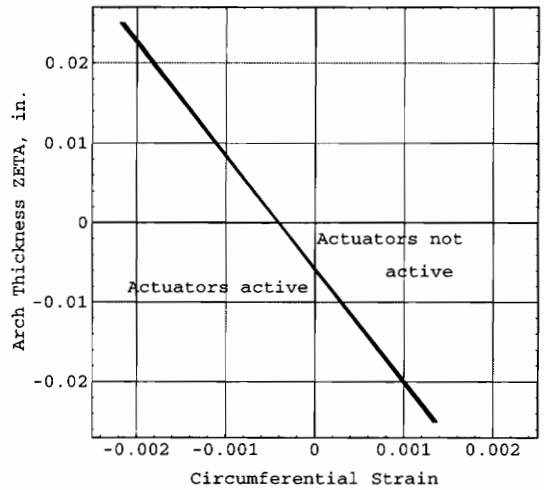

(b) Circumferential strains in the arch with and without the actuators

Figure 4.11 Circumferential stress and strain distribution through the thickness of the arch for equilibrium state S_1 (actuators active) and state S_4 (actuators not active), where each state has the same midspan displacement.

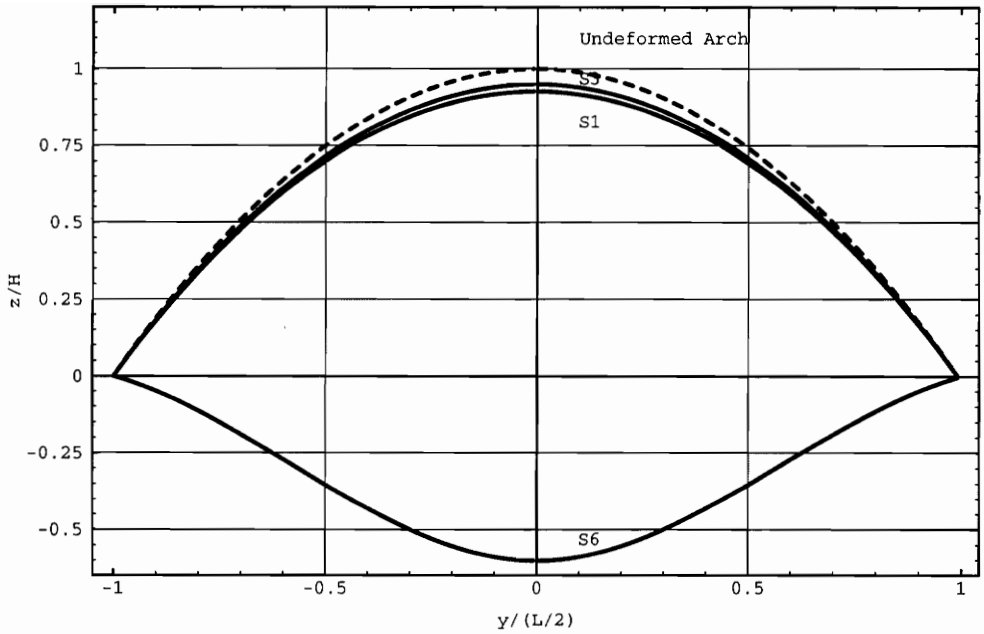

Figure 4.12 Mode shapes at specific equilibrium states along the lower elliptic path.

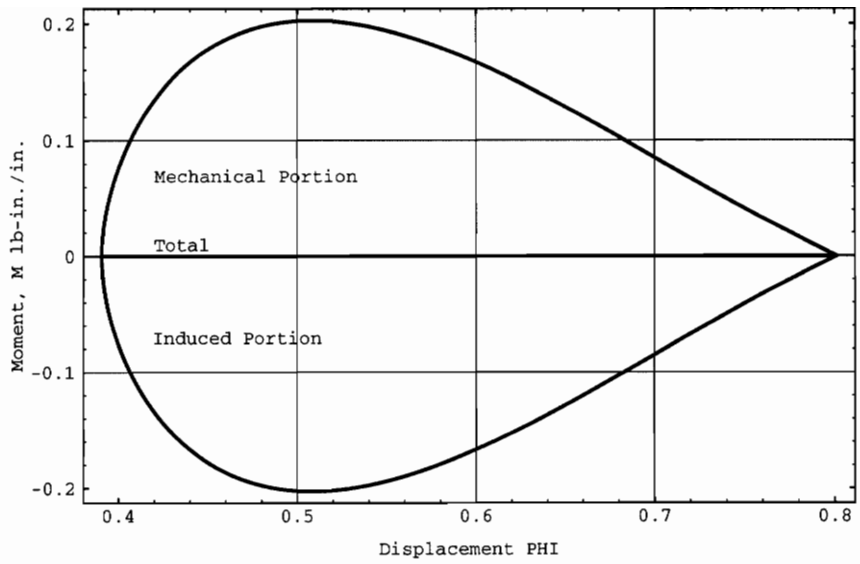

(a) Moments at *theta = beta* for load *P = 10.58 lbs/in* .

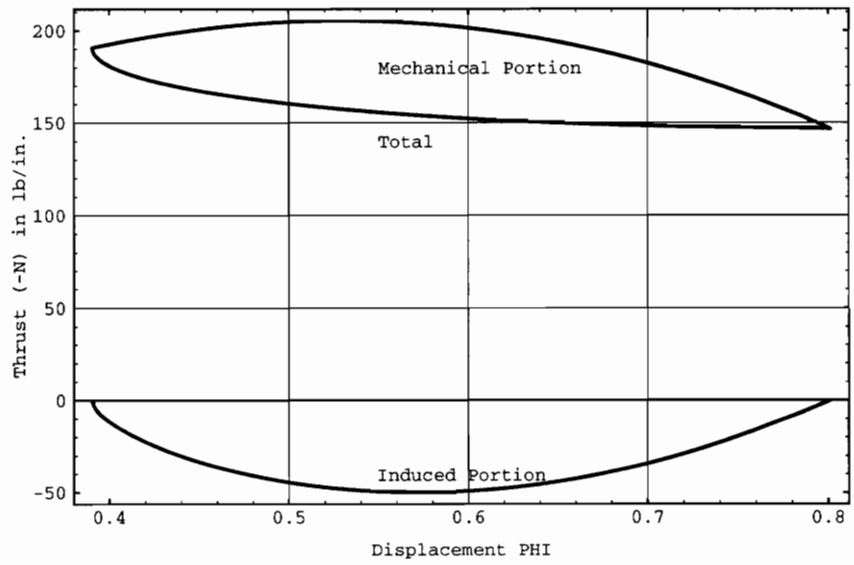

(b) Thrust along the alternate path

Figure 4.13 Effect of the actuators on the thrust and moments in the arch

induced thrust is negative, or tensile. The fact that negative induced strains (Figure 4.7) tend to cause a tensile stress resultant is explained by the ends of the arch remaining a fixed distance apart. Negative actuation strains tend to shorten the arc length, but this shortening is, to a large extent, prevented by the fixed end conditions. Thus, a negative actuation strain produces a tensile stress resultant rather than compressive because of the restraint provided by fixed ends. The combination of reduced total thrust and a positive equivalent end moments are stabilizing effects.

4.4. Parametric study

The actuation strains Λ_b and Λ_t obtained from the actuator load parameters e_a and e_b are functions of geometric parameters and material properties. For a given distribution of e_a and e_b, lower values of the actuation strains can be generated by selecting an appropriate geometry for the arch. The shallower the arch, the lower are the actuation strains that are needed to displace the arch to an inverted configuration in a stable manner. Similarly by selecting a suitable core material, the actuation strains can be lowered considerably. The sensitivities of the induced strains are computed relative to the baseline arch configuration (Table 4.1) and for the equilibrium state S_1 (Figure 4.8 and Table 4.2). The actuation load parameters have maximum magnitude in state S_1. First, sensitivities are computed for different ratios of the core thickness t_2 to the piezoelectric layer thickness t_1 for a constant total thickness $h = 2\ t_1 + t_2 = 0.05$ *inches*. Since the moduli of the piezoelectric layers and the core are the same in the baseline configuration, the arch rise parameter λ does not change from 2.10 if h remains constant at 0.05 inches.

4.4.1 Sensitivity of actuation strains to changes in thickness ratio t_2/t_1

For given values λ, R, β and Q_2/Q_1, a lower thickness ratio provides lower actuation

strains. This is shown in Figure 4.14a where the baseline value is indicated by the a dashed vertical line. Physically this implies that for a given actuator thickness, a thinner core requires lower actuation strains. However, the core can not be made too thin because of a minimum core thickness requirement for the actuators to function effectively. Notice that the bottom actuator strain has a higher magnitude than that in the top actuator.

4.4.2 Sensitivity of actuation strains to changes in elastic modulus ratio Q_2/Q_1

The elastic modulus plays an important role in determining the magnitude of the actuation strains. Lower actuation strains can be generated by selecting a core that is relatively softer than the PZT material. Thus for a given arch radius R, semi-opening angle β and a given actuator thickness, t_1, lower values of Q_2/Q_1 produce lower actuation strains as shown in Figure 4.14b. Again the baseline value is shown as a dashed vertical line. The core thickness t_2 acquires unique values for each distinct value of Q_2/Q_1, thereby keeping the value of λ constant. That is, t_2 changes as the ratio of Q_2/Q_1 changes to keep λ constant.

4.4.3 Sensitivity of actuation strains to changes in arch radius R and angle β

For assumed values of the thickness ratio, t_2/t_1, and the elastic modulus ratio, Q_2/Q_1, the effect of the semi- opening angle, β, and the arch radius, R, on the actuation strains is shown in Figure 4.15a and Figure 4.15b, respectively. The baseline value is shown as a dashed vertical line. Each point on Figures 4.15a and 4.15b is plotted for unique values of R and β. As β decreases, R increases. This is done to maintain a consistent value of λ for

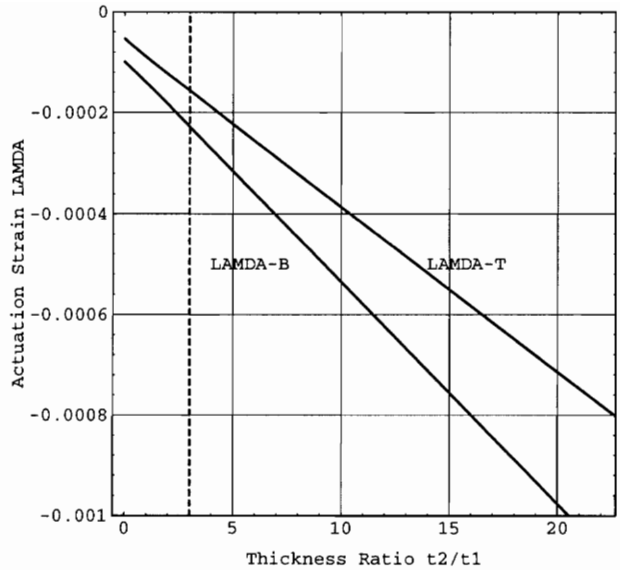

(a) Effect of thickness ratio on the PZT actuation strains

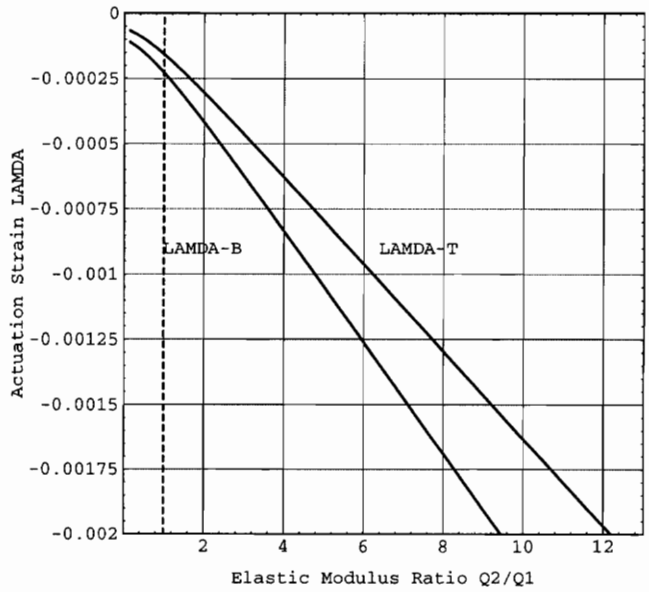

(b) Effect of elastic modulus ratio on the PZT actuation strains

Figure 4.14 Effect of the thickness ratio and elastic modulus ratio on the actuation strains for the equilibrium state S_1 (Ref. Table 4.1).

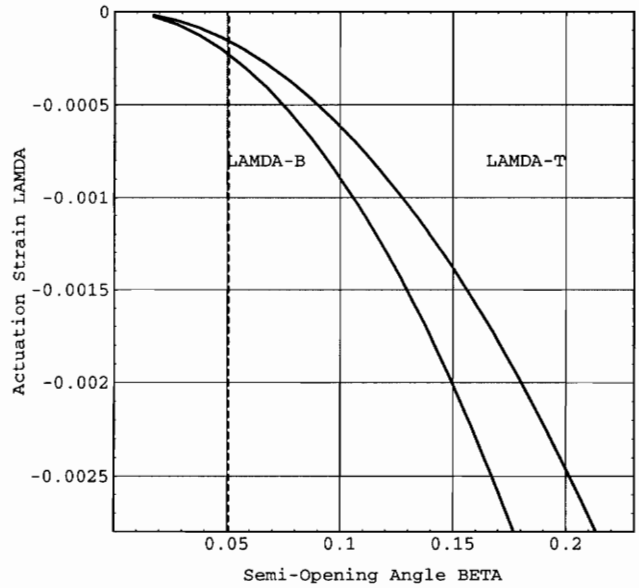

(a) Effect of semi-opening angle on the PZT actuation strains

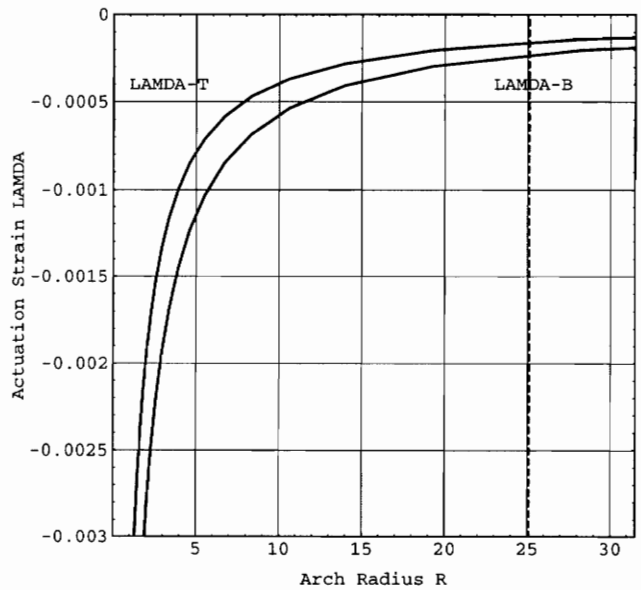

(b) Effect of arch radius on the PZT actuation strains

Figure 4.15 Effect of the semi-opening angle and the arch radius on the actuation strains for the equilibrium state S_1 (Ref. Table 4.1).

these plots. Figure 4.15a shows that for smaller values of β, the actuation strains are lower. Increasing the radius, R, of the arch also reduces the actuation strains. The physical implication of this is that by making the arch shallow, the values of Λ_b and Λ_t can be lowered.

5. Conclusion

5.1 Summary

An adaptive structure consisting of a shallow, circular cylindrical panel with piezoelectric material bonded to the concave and convex surfaces of a passive core material is proposed as an electromechanical nonlinear spring with a digital-like, force-displacement characteristic. The piezoelectric layers are polarized in the thickness direction such that a voltage applied across their thickness induces circumferential strains in the panel. The curved edges of the panel are free and the straight edges are pinned and remain a fixed distance apart. A spatially uniform, deadweight line load along the axial direction acts at midspan representing the load applied to the spring. The material laws for the piezoelectric

layers and the core material are linear elastic with the induced strains in the piezoelectric layers determined from the applied electric field. Strain-displacement relations are nonlinear. The response of the panel is independent of the axial coordinate and depends only on the circumferential coordinate. The governing ordinary differential equations for equilibrium and stability are derived using variational methods, and these equations are of the same form as for a shallow circular arch. Hence, both the terms panel and arch are used to describe this structure.

5.2 Concluding remarks

The response of the arch is geometrically nonlinear, and without induced strain actuators the arch exhibits snap-through instability under the midspan load. Consideration is limited to arch geometries such that snap-through occurs at a limit point on the load-displacement response plot. A procedure is developed to find induced strains distributions for the top and bottom actuators that displace the arch from a configuration at the limit point to an inverted configuration at the limit-point value of midspan load. By specifying various alternate equilibrium paths to the inverted state, actuator strain distributions are computed. This is an inverse formulation of the structural response problem, since the loads (induced strains) are determined for prescribed equilibrium states. Stability of the equilibrium states on the alternate equilibrium paths is inferred by evaluating the stability equation for buckling in a symmetric mode at each state. A value of zero for the stability equation indicates a critical equilibrium state. If the stability of the equilibrium states change, then the change in occurs at the critical points. All the results presented in this work are for a very shallow arch ($\lambda = 2.10$), where instability can occur only by buckling in a symmetric mode. We assume that the sign of the stability equation implies stability or instability of the equilibrium state for $\lambda = 2.10$.

It is shown that there exists induced actuation strain distributions that displace the arch

through stable equilibrium states to an inverted configuration. These distributions cause the thrust to decrease at a greater rate than the rate of increase in the midspan displacement. From a physical point of view, reducing the thrust in the arch through the induced strain actuators is a stabilizing influence. Also, it is found that the induced strain actuators tend to reduce the bending strains and stresses in the arch relative to comparable equilibrium states with the actuators not active.

Through parametric studies it is found that reduced actuation strain magnitudes (reduced actuator effort) occurs for a thicker piezoelectric layers relative to the core layer, and for a reduced core stiffness relative the piezoelectric layer stiffness. That is, actuator control is enhanced for thicker and stiffer piezoelectric layers relative to the core material.

5.3 Suggestions for future work

The parametric study presented here is limited. The following may merit further investigation:

- A more rigorous investigation of the stability of the equilibrium states, rather than merely monitoring the sign of the stability function, f.
- Deeper arches that exhibit snap-through at a bifurcation point on the primary path
- Lower load magnitudes (say, between the upper and lower limit points) for the alternate equilibrium paths in order to reduce induced strain magnitudes
- Softer support conditions for the arch, rather than fixed ends
- Shape memory alloys (SMA) actuators; since they have a larger force capacity than currently available piezoelectric materials, and they are frequently used for static control. However, SMAs have a slower dynamic response than the piezoelectric materials.

Finally, experimental validation of this study would lend greater credibility to it.

References

1. Seeley, C. E., Chattopadhyay, A., and Brei, D., "*Development of a Polymeric Piezoelectric C-Block Actuator Using Hybrid Optimization Technique*", AIAA Journal, Vol. 34, No. 1, January 1996, pp. 123-128.

2. NASA patent disclosure LAR 13729-1, 1988.

3. Carper, D. M., Johnson, E. R., and Hyer, *M. W., "Response of Composite Material Shallow Arch to Concentrated Load*", Journal of Aircraft, Vol. 23, No. 6, June 1986, pp. 529-536..

4. Biezeno, C. B. and Grammel, R., "*Engineering Dynamics*", Vol. 2, Blackie and Sons, London, 1956, p. 397.

5. Fung, Y. C. and Kaplan, A., *"Buckling of Low Arches or Curved Beams of Small Curvature"*, NACA, TN-2840, 1952.

6. Shreyer, H. L. and Masur, E. F., *"Buckling of Shallow Arches"*, Journal of Engineering Mechanics Division, ASCE, Vol. 92, 1966, pp. 1-17.

7. Shreyer, H. L., *"The Effect of Initial Imperfections on the Buckling Load of Shallow Circular Arches"*, Journal of Applied Mechanics, Vol. 39, 1972, p. 445.

8. Plaut, R. H., *"Influence of Load Position on the Stability of Shallow Arches"*, Z.A.M.P., Vol. 30, 1979, p. 548.

9. Plaut, R. H., *"Stability of Shallow Arches Under Multiple Loads"*, The Journal of Engineering Mechanics Division, October, 1978, pp. 1015-1026.

10. Plaut, R. H.., *"Postbuckling Analysis of Continuous, Elastic Systems Under Multiple Loads Part I: Theory"*, Joint ASME-CSME Applied Mechanics, Fluids Engineering and Bioengineering Conference, Niagara Falls, N. Y., June 1979, pp. 1-5.

11. Plaut, R. H., *"Postbuckling Analysis of Continuous, Elastic Systems Under Multiple Loads Part II: Applications"*, Joint ASME-CSME Applied Mechanics, Fluids Engineering and Bioengineering Conference, Niagara Falls, N. Y., June 1979, pp. 1-6.

12. Timoshenko, P. S., and Gere, J. M., *"Theory of Elastic Stability"*, 2nd Edition, McGraw-Hill Book Company, New York, 1961.

13. Simitses, G. J., *"An Introduction to the Elastic Stability of Structures"*, Robert E. Kreiger Publishing Inc., Florida, 1986, pp. 171-218.

14. Dym, C. L., "*Stability Theory and Applications to Structural Mechanics*", Noordhoff International Publishing-Leyden, 1974, pp. 144-166.

15. Rossi, A., Liang, C., and Rogers, C. A., "*Impedance Modeling of Piezoelectric Actuator Driven Systems:an Application to Cylindrical Ring Structures*", Proceedings of 34th SDM Conference, La Jolla, CA, 19-21 April, 1993, pp. 3618-3624.

16. Lalande, F., Chaudhry, Z., and Rogers, C. A., "*Modeling considerations for In-phase Actuation of Actuators bonded to Shell Structures*", Proceedings of 35th SDM Conference, Adaptive Structures Forum, Hilton Head, SC, April 1994, pp. 429-437

17. Chaudhry, Z., Rogers, C. A., and Lalande, F., "*Special considerations in the modeling of Induced Strain Actuator patches bonded to Shell Structures*", Smart Structures and Materials, SPIE, Orlando, Feb. 13 - 18, 1994, Vol. 2190, pp. 563 - 570.

18. Lalande, F., Chaudhry, Z., and Rogers, C. A., "*An experimental study of the Actuation Authority of Rings and Shells*", 36th AIAA/ASME/ASCE/AHS/ASC Structures, Structural Dynamics and Materials Conference and AIAA/ASME Adaptive Structures Forum, New Orleans, April 10 - 13, 1995.

19. Larson, P. H., and Vinson, J. R., " The use of Piezoelectric Materials in Curved Beams and Rings", Proceedings of the ASME Winter Annual Meeting, New Orleans, LA, 1993, pp. 277-285.

20. Niino, T., Egawa, S., Nishiguchi, N., and Higuchi, T., "*Development of an Electrostatic Actuator Exceeding 10N Propulsive Force*", Proceedings of the IEEE Micro Electro Mechanical Systems Workshop, Travemuende, Germany, Feb. 1992, pp. 122-127.

21. Egawa, S. and Higuchi, T., "*Multi-layered Electrostatic Film Actuator*", Proceedings of IEEE Micro Electro Mechanical Systems Workshop, Napa Valley, CA, Feb. 1990, pp. 166-171.

22. Bamford, R., Kuo, C. P., and Glaser, R., Wada, B. K., "*Long Stroke Precision Actuator*", Proceedings of the 36th AIAA/ASME/ASCE/AHS/ASC Structures, Structural Dynamics and Materials Conference, Part 5, New Orleans, LA, 1995, pp. 3278-3284.

23. "*Smart Skis and Other Adaptive Structures*", Mechanical Engineering, November 1995, pp. 77-81.

24. Wolfram, Stephen, "*Mathematica : A System for Doing Mathematics by Computer*", Second Edition, Addison-Wesley Publishing Company, 1993.

25. Carper, D., M, "*Large Deformation of Long Shallow Cylindrical Composite Panels*", Masters of Science Thesis, Engineering Mechanics, Virginia Polytechnic Institute and State University, Blacksburg, VA 24061, September, 1983.

Appendix A

The *Mathematica*™[24] (version 2.2) code for the solutions presented in section 2.4 to the governing equilibrium equations. In the *Mathematica* code that follows, Γ is replaced by x. Only input statements are given.

****** The governing ode, eq.(2.21), is ******

```
D[phi,{x,4}] + q^2 ( D[phi,{x,2}] + 1) == 0
```

The following equation (2.22) relates the thrust parameter q to the displacement, and is called the thrust relation:

```
q^2 = lam^4 (1/2 Integrate[(phi -(D[phi,x])^2/2),{x-1,1}]
        + ea)
```

****** The boundary conditions, eq.(2.23)******

```
bc1 = (phi/. x ->-1) == 0
```

```
bc2 = (D[phi,{x,2}]/. x -> -1) + eb ==0
bc3 = (phi/. x -> 1) == 0
bc4 = (D[phi,{x,2}]/. x -> 1) + eb == 0
```

****** The transition conditions, eq.(2.24), at x = 0 -point of load application ******

```
tr1 = (phi/. x ->0-) - (phi/. x->0+) == 0
tr2 = (D[phi,x]/. x -> 0-) - (D[phi,x]/. x ->0+)== 0
tr3 = (D[phi,{x,2}]/. x -> 0-) - (D[phi,{x,2}]/. x -> 0+) == 0
tr4 = (D[phi,{x,3}]/. x -> 0-) - (D[phi,{x,3}]/. x -> 0+) + p lam^4 == 0
```

**** Solution for $q \neq 0$, $q \neq \pi/2$, $q \neq \pi$ ****

****** The solution is of the form ******

******For -1 < x < 0******

```
phi1 = a1 + a2 x -x^2/2 + a3 Cos[q x] + a4 Sin[q x]
de = D[phi1,{x,4}] + q^2 (D[phi1,{x,2}] + 1)
Simplify[de]
```

******For 0 < x < 1******

```
phi2 = a5 + a6 x -x^2/2 + a7 Cos[q x] + a8 Sin[q x]
```

****** Applying boundary conditions and transition conditions ******

```
bc1 = phi1/. x-> -1
bc2 = (D[phi1,{x,2}] /. x -> -1) + eb
bc3 = phi2/. x-> 1
bc4 = (D[phi2,{x,2}] /. x -> 1) + eb
tr1 = (phi1/. x ->0) - (phi2/. x ->0)
tr2 = (D[phi1,x]/. x->0) - (D[phi2,x]/. x->0)
tr3 = (D[phi1,{x,2}]/. x -> 0) - (D[phi2,{x,2}]/. x -> 0)
tr4 = (D[phi1,{x,3}]/. x->0) - (D[phi2,{x,3}]/. x-> 0) +
      p lam^4
```

****** Solving for the coefficients ******

```
slv1 = Solve[{tr1 == 0,tr3 == 0},{a5,a7}]
a5 = a1; a7 = a3;
slv2 = Solve[tr4 == 0,a8]
a8 = a8/. slv2[[1]]
a8 = Simplify[a8]
slv3 = Solve[tr2 == 0,a6]
a6 = a6/. slv3[[1]]
a6 = Simplify[a6]
bc1
bc2
bc3
bc4
slv4 = Solve[{bc2 ==0, bc4 == 0},{a3,a4}]
a3 = a3/. slv4[[1,1]]
a4 = a4/. slv4[[1,2]]
Simplify[a3]
a3 = %;
Simplify[a4]
a4 = %;
slv5 = Solve[{bc1 == 0,bc3 == 0},{a1,a2}]
a1 = a1/. slv5[[1,1]]
Simplify[a1]
a1 = %;
a2 = a2/. slv5[[1,2]]
Simplify[a2]
a2 = %;
phi1
phi2
```

****** Solution to the equilibrium equation (eq.(2.54)) ******

```
Collect[phi1,p]
phi1 = %;
Collect[phi2,p]
phi2 = %;
```

****** Evaluation of the thrust (eq. (2.55))******

```
int1 = Integrate[(phi1 - (D[phi1,x])^2/2),{x,-1,0}]
int2 = Integrate[(phi2 - (D[phi2,x])^2/2),{x,0,1}]
thrust = q^2 - (lam^4/2)(int1 + int2) - lam^4 ea
Together[thrust]
thrust = Numerator[Together[thrust]]
```

**** Solution for q = π /2 ****

****** The solution is of the form ******

******For -1 < x < 0******

```
phi1 = a1 + a2 x -x^2/2 + a3 Cos[q x] + a4 Sin[q x]
de = D[phi1,{x,4}] + q^2 (D[phi1,{x,2}] + 1)
Simplify[de]
```

******For 0 < x < 1******

```
phi2 = a5 + a6 x -x^2/2 + a7 Cos[q x] + a8 Sin[q x]
```

****** Applying boundary and transition conditions ******

```
q = Pi/2;
bc1 = phi1/. x-> -1
bc2 = (D[phi1,{x,2}] /. x -> -1) + eb
bc3 = phi2/. x-> 1
bc4 = (D[phi2,{x,2}] /. x -> 1) + eb
tr1 = (phi1/. x ->0) - (phi2/. x ->0)
```

```
tr2 = (D[phi1,x]/. x->0) - (D[phi2,x]/. x->0)
tr3 = (D[phi1,{x,2}]/. x -> 0) - (D[phi2,{x,2}]/. x -> 0)
tr4 = (D[phi1,{x,3}]/. x->0) - (D[phi2,{x,3}]/. x-> 0) + p lam^4
```

****** Solving for the coefficients ******

```
slv1 = Solve[bc2 ==0,a4]
a4 = a4/. slv1[[1]]
a7 = a3;
slv2 = Solve[bc4 == 0,a8]
a8 = a8/. slv2[[1]]
bc1
bc3
tr1
tr2
tr4
a5 = a1;
slv3 = Solve[{bc1 == 0,bc3 == 0,tr2==0},{a1,a2,a6}]
a1 = Simplify[a1/. slv3[[1,1]]]
a2 = a2/. slv3[[1,2]]
a6 = a6/. slv3[[1,3]]
```

****** Solution to the equilibrium equation (eq.(2.69)) ******

```
phi1
phi2
```

****** Evaluation of the thrust (eq. (2.70))******

```
int1 = Integrate[(phi1 - (D[phi1,x])^2/2),{x,-1,0}]
int2 = Integrate[(phi2 - (D[phi2,x])^2/2),{x,0,1}]
thrust = q^2 - (lam^4/2)(int1 + int2) - lam^4 ea
Together[thrust]
```

****** Solution for $q = \pi$ ******

```
*** The solution is of the form ***
***For -1 < x < 0***
phi1 = a1 + a2 x -x^2/2 + a3 Cos[q x] + a4 Sin[q x]
de = D[phi1,{x,4}] + q^2 (D[phi1,{x,2}] + 1)
Simplify[de]
***For 0 < x < 1***
phi2 = a5 + a6 x -x^2/2 + a7 Cos[q x] + a8 Sin[q x]
*** Applying boundary and transition conditions ***
q = Pi;
bc1 = phi1/. x-> -1
bc2 = (D[phi1,{x,2}] /. x -> -1) + eb
bc3 = phi2/. x-> 1
bc4 = (D[phi2,{x,2}] /. x -> 1) + eb
tr1 = (phi1/. x ->0) - (phi2/. x ->0)
tr2 = (D[phi1,x]/. x->0) - (D[phi2,x]/. x->0)
tr3 = (D[phi1,{x,2}]/. x -> 0) - (D[phi2,{x,2}]/. x -> 0)
tr4 = (D[phi1,{x,3}]/. x->0) - (D[phi2,{x,3}]/. x-> 0) +
    p lam^4
*** Solving for the coefficients ***
slv1 = Solve[bc2 == 0,a3]
a3 = a3/. slv1[[1]]
slv2 = Solve[bc4 == 0,a7]
a7 = a7/. slv2[[1]]
tr3
bc1
bc3
tr1
tr2
tr4
```

```
a5 = a1;
tr24 = Simplify[Pi^2 tr2 + tr4]
tr42 = Simplify[ Pi^2 tr2 - tr4]
bc1
bc3
tr1
slv3 = Solve[{bc1 == 0,bc3 ==0,tr24 == 0},{a1,a2,a6}]
a1 = Simplify[a1/. slv3[[1,1]]]
a2 = a2/.slv3[[1,2]]
a6 = a6/. slv3[[1,3]]
tr42
a4 = b + s
a8 = b - s
Simplify[tr42]
slv4 = Solve[tr42 == 0,s]
s = s/. slv4[[1]]
```

****** Solution to the equilibrium equation (eq.(2.71)) ******

```
phi1
phi2
Simplify[bc1]
bc2
Simplify[bc3]
bc4
tr1
Simplify[tr2]
tr3
Simplify[tr4]
```

****** Evaluation of the thrust (eq. (2.72))******

```
int1 = Integrate[(phi1 - (D[phi1,x])^2/2),{x,-1,0}]
```

```
int2 = Integrate[(phi2 - (D[phi2,x])^2/2),{x,0,1}]
thrust = q^2 - (lam^4/2)(int1 + int2) - lam^4 ea
Together[thrust]
thrust = Numerator[Together[thrust]]
Together[phi2/. x->0]
thrust/.{eb ->0,ea ->0}
check1 = thrust/.{eb ->0,ea ->0,b ->0}
```

Appendix B

The *Mathematica*™(24) (version 2.2) code for solutions presented in section 2.5 to the stability equations. In the *Mathematica* code that follows, Γ is replaced by x. Only input statements are given.

****** Equilibrium displacement, eq.(2.54) ******

******For -1 < x < 0******

```
phi1 = 1/2 + q^(-2) - eb/q^2 - x^2/2 - (Cos[q*x]*Sec[q])/q^2 +
        (eb*Cos[q*x]*Sec[q])/q^2 +
        p*(-lam^4/(2*q^2) - (lam^4*x)/(2*q^2) +
        (lam^4*Sin[q*x])/(2*q^3) + (lam^4*Cos[q*x]*Tan[q])/(2*q^3))
```

******For 0 < x < 1******

```
phi2 = 1/2 + q^(-2) - eb/q^2 - x^2/2 - (Cos[q*x]*Sec[q])/q^2 +
```

```
(eb*Cos[q*x]*Sec[q])/q^2 +
p*(-lam^4/(2*q^2) + (lam^4*x)/(2*q^2) -
(lam^4*Sin[q*x])/(2*q^3) + (lam^4*Cos[q*x]*Tan[q])/(2*q^3))
```

****** Particular solution to the stability equation for the second derivative of the additional displacement at buckling; called y[x]. Based on the method of variation of parameters.******

```
v11 = - q1^2 Integrate[Cos[q x] (1 + D[phi1,{x,2}]),x]/q
v12 = - q1^2 Integrate[Cos[q x] (1 + D[phi2,{x,2}]),x]/ q
v21 = q1^2 Integrate[Sin[q x] (1 + D[phi1,{x,2}]),x]/q
v22 = q1^2 Integrate[Sin[q x] (1 + D[phi2,{x,2}]),x]/q
yp1 = v11 Sin[q x] + v21 Cos[q x]
Simplify[%]
yp1 = %;
yp1 = (q1^2*Sec[q]*(-2*q*Cos[q*x] + 2*eb*q*Cos[q*x] -
      2*lam^4*p*q*x*Cos[q + q*x] - 4*q^2*x*Sin[q*x] +
      4*eb*q^2*x*Sin[q*x] + lam^4*p*Sin[q + q*x]))/(8*q^3)
```

****** Check if yp1 satisfies ode on the left side. ******

```
de1 = D[yp1,{x,2}] + q^2 yp1 + q1^2 (1 + D[phi1,{x,2}])
Simplify[%]
yp2 = Simplify[v12 Sin[q x] + v22 Cos[q x]]
yp2 = (q1^2*Sec[q]*(-2*q*Cos[q*x] + 2*eb*q*Cos[q*x] +
       2*lam^4*p*q*x*Cos[q - q*x] - 4*q^2*x*Sin[q*x] +
      4*eb*q^2*x*Sin[q*x] + lam^4*p*Sin[q - q*x]))/(8*q^3)
```

****** Check if yp2 satisfies ode on the right side. ******

```
de2 = D[yp2,{x,2}] + q^2 yp2 + q1^2 (1 + D[phi2,{x,2}])
Simplify[%]
```

****** The total solution of the ode for the second derivative of the additional displacement is y1 on the left and y2 on the right.******

```
y1 = c11 Sin[q x] + c12 Cos[q x] + yp1
```

```
y2 = c21 Sin[q x] + c22 Cos[q x] + yp2
```

****** Continuity conditions for the second derivative solution to determine relations between constants c11, c12, c21, and c22. ******

```
tr1 = (y1/. x ->0) - (y2/. x->0)
Clear[c12,c22];c12 = k2; c22 = k2;
tr2 = (D[y1,x]/. x ->0) - (D[y2,x]/. x->0)
c11 = k1 + b1;c21 = k1 -b1;tr2 = Simplify[tr2]
s1 = Solve[tr2 == 0,b1]
b1 = b1/. s1[[1]]
y1
y2
```

****** With the second derivative of the buckling displacement determined up to two unknown constants, we integrate twice to get the displacement. Then, impose continuity conditions. ******

```
dphi11 = Integrate[y1,x] + c13
phi11 = Integrate[dphi11,x] + c14
dphi12 = Integrate[y2,x] + c23
phi12 = Integrate[dphi12,x] + c24
tr3 = (phi11/. x -> 0) - (phi12/. x ->0)
c14 = k4; c24 = k4;
tr4 = (dphi11/. x ->0) - (dphi12/. x -> 0)
Simplify[%]
c13 = k3 + b3; c23 = k3 - b3; tr4 = Simplify[tr4]
s2 = Solve[tr4 == 0,b3]
b3 = b3/. s2[[1]]
phi11
phi12
```

****** Checking that the buckling modes satisfy the governing ode and continuity conditions at x = 0. ******

```
ode1 = D[phi11,{x,4}] + q^2 D[phi11,{x,2}] + q1^2 (1 + D[phi1,{x,2}])
Simplify[%]
ode2 = D[phi12,{x,4}] + q^2 D[phi12,{x,2}] + q1^2 (1 + D[phi2,{x,2}])
Simplify[%]
phi11/. x ->0
phi12/. x ->0
D[phi11,x]/. x ->0
D[phi12,x]/. x ->0
Simplify[(D[phi11,x]/. x ->0) - (D[phi12,x]/. x ->0)]
Simplify[(D[phi11,{x,2}]/. x ->0) - (D[phi12,{x,2}]/. x ->0)]
Simplify[(D[phi11,{x,3}]/. x ->0) - (D[phi12,{x,3}]/. x ->0)]
```

******Coefficients of k1, k2, k3 and k4 for phi11 and phi12 ******

```
g11 = Simplify[phi11/.{k1 ->1,k2->0,k3->0,k4->0,q1->0}]
g21 = Simplify[phi12/.{k1 ->1,k2->0,k3->0,k4->0,q1->0}]
g12 = Simplify[phi11/.{k1 ->0,k2->1,k3->0,k4->0,q1->0}]
g22 = Simplify[phi12/.{k1 ->0,k2->1,k3->0,k4->0,q1->0}]
g13 = Simplify[phi11/.{k1 ->0,k2->0,k3->1,k4->0,q1->0}]
g23 = Simplify[phi12/.{k1 ->0,k2->0,k3->1,k4->0,q1->0}]
g14 = Simplify[phi11/.{k1 ->0,k2->0,k3->0,k4->1,q1->0}]
g24 = Simplify[phi12/.{k1 ->0,k2->0,k3->0,k4->1,q1->0}]
g15 = Simplify[phi11/.{k1 ->0,k2->0,k3->0,k4->0,q1->1}]
g25 = Simplify[phi12/.{k1 ->0,k2->0,k3->0,k4->0,q1->1}]
a1 = (lam^4/2)( Integrate[(g11 - D[phi1,x] D[g11,x]),{x,-1,0} ] +
            Integrate[(g21 - D[phi2,x] D[g21,x]),{x,0,1}  ]  )
a2 = (lam^4/2)( Integrate[(g12 - D[phi1,x] D[g12,x]),{x,-1,0} ] +
            Integrate[(g22 - D[phi2,x] D[g22,x]),{x,0,1}  ]  )
Simplify[a2]
a2 = %;
a3 = (lam^4/2)( Integrate[(g13 - D[phi1,x] D[g13,x]),{x,-1,0} ] +
```

```
            Integrate[(g23 - D[phi2,x] D[g23,x]),{x,0,1}  ]  )
a4 = (lam^4/2)( Integrate[(g14 - D[phi1,x] D[g14,x]),{x,-1,0} ] +
            Integrate[(g24 - D[phi2,x] D[g24,x]),{x,0,1}  ]  )
a5 = (lam^4/2)( Integrate[(g15 - D[phi1,x] D[g15,x]),{x,-1,0}] +
            Integrate[(g25 - D[phi2,x] D[g25,x]),{x,0,1}]);
Simplify[%];
a5 = %;
```

****** Boundary conditions applied and equations written in matrix form. ******

```
b11=.;b12=.;b13=.;b21=.;b22=.;b23=.;b31=.;b32=.;b33=.;
bMatrix = {{b11,b12,b13},{b21,b22,b23},
        {b31,b32,b33}};MatrixForm[bMatrix]
b11 = g12/.x->-1
b21 = D[g12,{x,2}]/.x->-1
b31 = a2;
b12 = 1;
b22 = 0;
b32 = lam^4;
b13 = g15/.x->-1
b23 = D[g15,{x,2}]/.x->-1
b33 = a5 -1
```

****** Characteristic equation; stability equations for symmetric buckling mode eq. (2.83). ******

```
ceqn = Det[bMatrix]
Length[ceqn]
Exponent[ceqn,eb]
c20 = Coefficient[ceqn, p^2]/. eb ->0
Length[c20]
c11 = Coefficient[ceqn, p eb]
```

```
Length[c11]
c02 = Coefficient[ceqn, eb^2]/.p->0
Length[c02]
c10 = Coefficient[ceqn, p]/.eb->0
Length[c10]
c01 = Coefficient[ceqn,eb]/. p->0
Length[c01]
c00 = ceqn/. {p->0, eb ->0}
Length[c00]
Length[c20]+Length[c11]+Length[c02]+Length[c10]+Length[c01]+
Length[c00]
```

Vita

The author was born in Amritsar, India to Indu and Harjit Singh on 29th of April, 1972. After completing his Bachelor of Engineering degree in Mechanical Engineering from Osmania University, India in 1994, he furthered his education through graduate studies at Virginia Tech. He completed the Masters of Science degree in Aerospace Engineering in 1996.